ABSOLUTE OSCILLATOR STRENGTHS FOR IRON, COPPER, CADMIUM AND GOLD MEASURED BY THE ATOMIC BEAM METHOD

Thesis by

Robert Carl Ashenfelter

In Partial Fulfillment of the Requirements

For the Degree of

Doctor of Philosophy

California Institute of Technology

Pasadena, California

1967

(Submitted May 25, 1967)

ACKNOWLEDGMENTS

I gratefully acknowledge the guidance and advise of Professor Robert B. King under whose supervision this research was carried out.

Much of the apparatus and many of the techniques used in the experiment were developed by those who previously worked on this project: M. H. Davis, G. D. Bell, G. M. Lawrence, and J. K. Link.

This research was supported by the office of Naval Research under Contract Nonr 200(49).

ABSTRACT

Absolute f-values for 7 transitions in the first spectra of 4 elements have been measured using the atomic beam absorption technique. The equivalent widths of the absorption lines are measured with a photoelectric scanner and the atomic beam density is determined by continuously weighing a part of it with a sensitive automatic microbalance. The complete theory is presented and corrections are calculated to cope with gas adsorption by the deposit on the microbalance pan and atoms which do not stick to the pan. An additional correction for the failure of the assumption of effusive flow in the formation of the atomic beam at large densities has been measured experimentally.

The following f-values were measured:

Fe: $f_{\lambda 3720} = 0.0430 \pm 8\%$

Cu: $f_{\lambda 3247} = 0.427 \pm 4.5\%$, $f_{\lambda 3274} = 0.206 \pm 4.7\%$, $f_{\lambda 2492} = 0.0037 \pm 9\%$

Cd: $f_{\lambda 3261} = 0.00190 \pm 7\%$, $f_{\lambda 2288} = 1.38 \pm 12\%$

Au: $f_{\lambda 2428} = 0.283 \pm 5.3\%$

Comparison with other accurately measured f-values, where they exist, shows agreement within experimental errors.

CONTENTS

TABLES

FIGURES

I INTRODUCTION

The oscillator strength, or f-value, of an atomic transition is a measure of the rate at which atoms absorb electromagnetic energy. If each atom which is capable of undergoing the transition is replaced by a "classical oscillator" consisting of an electron with an elastic restoring force such that it has the same resonant frequency as the original atomic transition, the absorption is easily calculated classically. The ratio of the energy actually absorbed by the atoms to that absorbed by classical oscillators is defined to be the f-value of the atomic transition.

In astrophysics, f-values are used to determine the abundances of elements in the solar atmosphere and in stellar atmospheres. Laboratory uses include measurements of the density and temperature of radiating atoms in plasmas and hot gases such as those produced by arcs and shock tubes.

Oscillator strengths may be obtained theoretically if the electric dipole (or higher multipole for forbidden lines) matrix elements can be calculated. Because small errors in the wave functions of the initial and final states can lead to large errors in the matrix elements, accurate f-values can be calculated only for simple atoms such as hydrogen and helium. For other elements, f-values are obtained from approximate calculations or they are measured experimentally. E. W. Foster[1] has described most of the important experimental methods.

The f-values reported here were measured with an atomic beam apparatus. The element under investigation is placed in a crucible inside a vacuum chamber and heated to a temperature at which it vaporizes. Atoms effuse out of a small orifice in the crucible forming an atomic beam the angular dimensions of which are defined by suitably placed knife edges. A light beam from a continuum source passes through the atomic beam and into a spectrograph where it is analyzed to determine the total absorption of the spectral line being measured. At the same time the density of the atomic beam is monitored by weighing a part of the beam which deposits on a microbalance pan. From these measurements and the temperature of the crucible, the f-value can be determined. This method is limited to reasonably strong spectral lines of neutral atoms arising from low-lying energy levels which are populated at the temperature of the crucible.

The atomic beam method was first used by Wessel[2] and Kopfermann and Wessel[3] to measure f-values of Ba and Fe. Under the supervision of Professor Robert B. King at the California Institute of Technology, an atomic beam apparatus was constructed by M. H. Davis.[4] Oscillator strengths of Cu, Fe, Mn, and Cr were measured with this apparatus and published by Bell, Davis, King, and Routly.[5,6,7] In these measurements the absorption was measured with photographic plates and the atomic beam density with a sensitive quartz fiber spring balance. Bell and King[8] also measured an f-value of Pb using a manually balanced electrobalance to more accurately measure the atomic beam flux.

Major improvements in the apparatus were made by G. M. Lawrence and J. K. Link.[9,10,11] They used a photoelectric scanner mounted in the camera holder of the spectrograph instead of photographic plates to measure the amount of the absorption. In addition an automatically balancing electrobalance was used to continuously record the mass deposited by the atomic beam. Oscillator strengths of Cr, Co, Ni, Ga, Pd, Ag, In, Sn, Au, and Tl were measured with this apparatus.

The present work is a continuation of this project. A new, more sensitive, photoelectric scanner allows more accurate measurements of the weak absorption lines. The automatically recording microbalance has also been improved. These refinements make it possible to measure smaller f-values and to measure large ones more accurately.

II THEORY

The theory of the formation of absorption lines in an atomic beam was derived by Davis.[4] The following derivation leads to similar results with the exception of the introduction of the parameter a'.

A. Atomic Beam Distribution

The geometry of the atomic beam and the coordinate system which will be used is shown in Figure 1. It is assumed that the distribution of atoms in the beam is given by the kinetic theory of gases for effusive flow through an orifice and that the size of the orifice is small enough that it can be treated as a point source. The validity of these assumptions is discussed elsewhere.

The number of atoms per second flowing through the orifice at an angle θ from the normal, per unit solid angle, with speeds between v and v + dv, is given by Kennard[12] as

$$\mathcal{N}_v(\theta)\, dv = K \beta^3 v^3 e^{-\beta^2 v^2} \cos\theta\, dv \qquad (1)$$

where

$$\beta = \sqrt{M/2RT} \qquad (2)$$

with M the atomic mass of the atoms, R the gas constant, and T the absolute temperature of the crucible. The constant K is related to the density n_o of atoms inside the crucible and the area of the orifice σ by

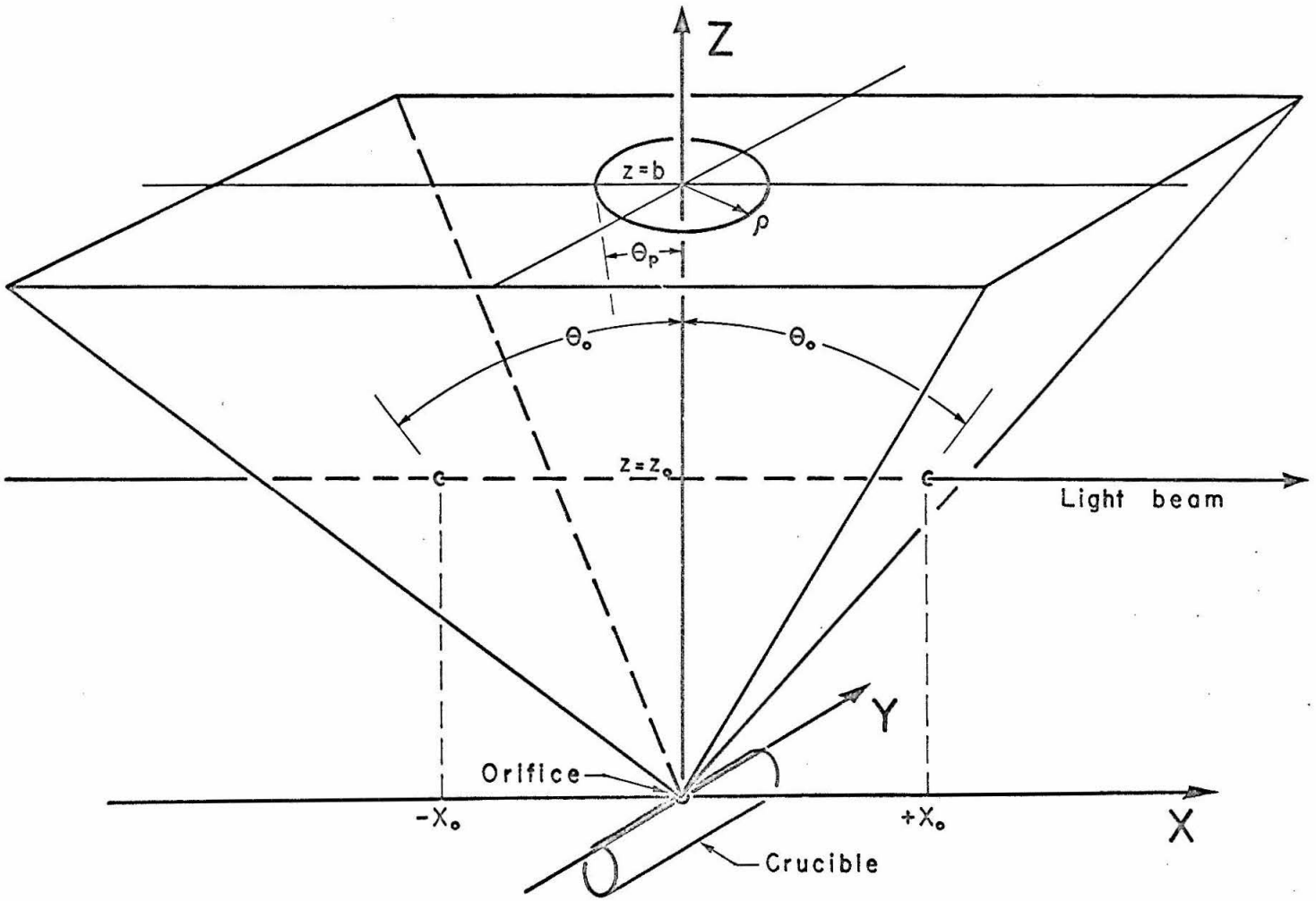

Figure 1. Atomic beam geometry.

$$K = \pi^{-3/2} \sigma n_o \quad . \tag{3}$$

At any point in the atomic beam the density of atoms with speeds between v and v + dv is

$$n_v(r,\theta)dv = \frac{\mathcal{N}_v(\theta)}{vr^2} dv = K \frac{\beta^3 v^2}{r^2} e^{-\beta^2 v^2} \cos\theta \, dv \tag{4}$$

where r is the distance from the orifice.

The light beam passes through the atomic beam at a height z_o above the orifice and is assumed to have negligible cross section. The quantity which will be needed is $N_{v_x}(z_o)dv_x$, the number of atoms per unit area with x-component of velocity between v_x and $v_x + dv_x$ as seen looking along the light beam. Substituting $r = z_o \sec\theta$ and $v = v_x \csc\theta$ into equation (4) yields the density distribution along the light path:

$$n_{v_x}(z_o,\theta)dv_x = K \frac{\beta^3 v_x^2}{z_o^2} e^{-\beta^2 v_x^2 \csc^2\theta} \cot^3\theta \, dv_x \, . \tag{5}$$

This equation must be integrated from $-x_o$ to $+x_o$ to give $N_{v_x}(z_o)dv_x$. Consider the case $v_x > 0$; the integral will run from 0 to $+x_o$ only, since for negative x, no atoms have positive x-velocities:

$$N_{v_x}(z_o) = \int_0^{x_o} K \frac{\beta^3 v_x^2}{z_o^2} e^{-\beta^2 v_x^2 \csc^2\theta} \cot^3\theta \, dx \, . \tag{6}$$

With the substitutions $dx = z_o \sec\theta \, d\theta$ and then $u = \csc^2\theta$, the

integral can be done. The result is

$$N_{v_x}(z_o) = K \frac{\beta}{2z_o} e^{-(\beta \csc \theta_o)^2 v_x^2} \quad . \qquad (7)$$

Although this result was calculated for $v_x > 0$, the same result is obtained for $v_x < 0$, so equation (7) holds for all values of v_x.

B. Atomic Absorption

Since equation (7) has the same form as the Maxwellian velocity distribution for one component of velocity, the following theory closely parallels the theory of the formation of absorption lines by a monatomic gas. See, e.g., Unsöld[13] pp. 288 ff. or Aller[14] pp. 322 ff.

The absorption coefficient per atom as a function of frequency ν is given by the Weisskopf-Wigner formula:

$$\alpha_\nu = \frac{\pi e^2}{mc} f \frac{(\Gamma/4\pi^2)}{(\nu_o - \nu)^2 + (\Gamma/4\pi)^2} \qquad (8)$$

where f is the oscillator strength of the absorption line centered at ν_o, e and m are the charge and mass of an electron, c the velocity of light, and Γ is the radiation damping constant of the line. If the atom is moving, the center of the line is Doppler shifted from ν_o to $\nu_o + \nu_o v_x/c$ so equation (8) becomes

$$\alpha_\nu = \frac{\pi e^2}{mc} f \frac{(\Gamma/4\pi^2)}{(\nu_o + \nu_o v_x/c - \nu)^2 + (\Gamma/4\pi)^2} \quad . \qquad (9)$$

The optical depth τ_ν is obtained by multiplying equation (9) by $N_{v_x}(z_o)$ and integrating over v_x:

$$\tau_\nu = K \frac{\beta}{2z_o} \frac{\pi e^2}{mc} f \int_{-\infty}^{+\infty} \frac{(\Gamma/4\pi^2)\ e^{-(\beta \csc \theta_o)^2 v_x^2}}{(\nu_o + \nu_o v_x/c - \nu)^2 + (\Gamma/4\pi)^2}\ dv_x . \quad (10)$$

This integral is conventionally written as

$$\tau_\nu = C\, H(a',u) \quad (11)$$

where the following substitutions have been made:

$$C = K \frac{\beta}{2z_o} \frac{\pi e^2}{mc} f \frac{c}{\nu_o} \quad (12)$$

$$H(a',u) = \frac{1}{\pi} \int_{-\infty}^{+\infty} \frac{a'\, e^{-y^2}}{a'^2 + (u - y)^2}\ dy \quad (13)$$

$$a' = \frac{\Gamma/4\pi}{\Delta\nu_D'} = \text{damping ratio} \quad (14)$$

$$u = \frac{\nu - \nu_o}{\Delta\nu_D'} \quad (15)$$

$$y = \frac{\nu_o}{\Delta\nu_D'} \frac{v_x}{c} \quad (16)$$

$$\Delta\nu_D' = \frac{\nu_o}{\beta c} \sin\theta_o = \frac{\nu_o}{c} \sqrt{2RT/M} \sin\theta_o = \text{Doppler width} \quad (17)$$

The Doppler width and damping ratio are primed to distinguish them from the corresponding quantities with $\sin\theta_o$ removed which arise

in the theory of absorption by a gas.

The intensity I_ν of the transmitted light is given by

$$I_\nu = I_o \, e^{-\tau_\nu} = I_o \, e^{-C\,H(a',u)} \tag{18}$$

where I_o is the intensity of the incident light.

C. The Curve of Growth

Since the width of the line profile given by equation (18) is much smaller than the resolution of the spectrograph which is used, a measure of the total amount of light absorbed is needed. This quantity is the "equivalent width" defined as

$$W_\nu = \int_{\text{line}} \frac{I_o - I_\nu}{I_o} \, d\nu \quad . \tag{19}$$

Using equation (18) this becomes

$$W_\nu = \int_{-\infty}^{+\infty} \left\{ 1 - e^{-C\,H(a',u)} \right\} \Delta \nu_D' \, du \tag{20}$$

where the limits of integration have been extended to $\pm \infty$.

At this point it is convenient to express the formulas in terms of wavelength $\lambda = c/\nu$ instead of frequency ν because the experimental measurements are made in terms of λ. Since the absorption lines are very narrow, no error is made in setting

$$(\nu - \nu_o) = \frac{c}{\lambda_o^2} (\lambda - \lambda_o) \quad . \tag{21}$$

This equation also applies if $(\nu - \nu_o)$ is replaced by $\Delta\nu_D'$ or W_ν with $(\lambda - \lambda_o)$ replaced by the respective quantity in wavelength units. With these changes, equation (20) becomes

$$\frac{W_\lambda}{\Delta\lambda_D'} = \int_{-\infty}^{+\infty} \left\{1 - e^{-C\,H(a',u)}\right\} du \qquad (22)$$

where

$$\Delta\lambda_D' = \frac{\lambda_o}{c}\sqrt{2RT/M}\,\sin\theta_o \qquad (23)$$

$$C = K\frac{\beta}{2z_o}\frac{\pi e^2}{mc} f\,\lambda_o \qquad (24)$$

$$a' = \frac{\lambda_o^2\,\Gamma}{4\pi c\,\Delta\lambda_D'} \quad . \qquad (25)$$

In addition equations (11), (15), (16), (18), and (19) are valid if every ν, $\Delta\nu_D'$, W_ν, etc. is replaced by λ, $\Delta\lambda_D'$, W_λ, etc.

For the lines considered in this work the parameter a' can be expressed in terms of the f-value. The damping constant can be written as (see Aller[14] pp. 172-176)

$$\Gamma = \Gamma_u + \Gamma_\ell \qquad (26)$$

where for any state i,

$$\Gamma_i = \frac{1}{\tau_i} = \sum_j A_{ij} \qquad (27)$$

and

$$A_{ij} = \frac{8\pi^2 e^2}{mc\,\lambda_{ij}^2}\,\frac{g_j}{g_i}\,f_{ji} \quad . \tag{28}$$

The subscripts u and ℓ refer to the upper and lower energy levels for the transition under consideration, τ_i is the lifetime of the state i, A_{ij} is the Einstein coefficient for spontaneous transitions from state i to j, g_i is the statistical weight of level i and is equal to $(2J + 1)$, and f_{ji} is the absorption oscillator strength for the transition $j \rightarrow i$ which has been and will henceforth be referred to simply as f. The summation in equation (27) extends over all levels j that are below level i. For the transitions under consideration, level ℓ is either the ground state or in any case has $\tau_\ell \gg \tau_u$ so that Γ_ℓ can be neglected. Also, the only term in the summation that is important is $A_{u\ell}$, i.e. the A-value for the line being investigated. With these restrictions, equations (26), (27), and (28) can be combined and substituted into equation (25) to give

$$a' = \frac{2\pi e^2}{mc^2\,\Delta\lambda_D'}\,\frac{g_\ell}{g_u}\,f \quad . \tag{29}$$

For special case $a' = 0$, it can be shown that equation (13) simplifies to

$$H(0,u) = e^{-u^2} \tag{30}$$

and equation (22) becomes

$$\frac{W_\lambda}{\Delta\lambda_D'} = \int_{-\infty}^{+\infty} \left\{ 1 - \exp\left(C\, e^{-u^2}\right) \right\} du \quad . \qquad (31)$$

If the exponential is expanded in a Taylor's series the integral can be evaluated term by term giving

$$\frac{W_\lambda}{\Delta\lambda_D'} = \sqrt{\pi} \left\{ C - \frac{C^2}{2!\sqrt{2}} + \frac{C^3}{3!\sqrt{3}} - + \ldots \right\} \quad . \qquad (32)$$

Unsöld[13] p. 290 also gives an asymptotic expansion which is useful for large C.

The relation between $W_\lambda/\Delta\lambda_D'$ and C given by equations (22) or (32) is known as the curve of growth. It shows how the strength of the absorption line varies with the number of absorbing atoms. Moise[15] App. C gives tables of the curve of growth for various values of the damping ratio. Figure 2, plotted from these tables, shows the form of the curve of growth for various values of a'. The portion of the curve for $C \lesssim 1/2$ is known as the linear part. For intermediate values of C the curve flattens out and becomes dependent on a'. For large C the curve approaches the asymptote $W_\lambda/\Delta\lambda_D' = 2\sqrt{\sqrt{\pi}\, a'\, C}$.

Experimentally, values of C are obtained from the curve of growth and the measured values of W_λ. As the slope of the curve decreases, effects of errors in W_λ are magnified and so it is desirable to obtain data on the linear part of the curve. However

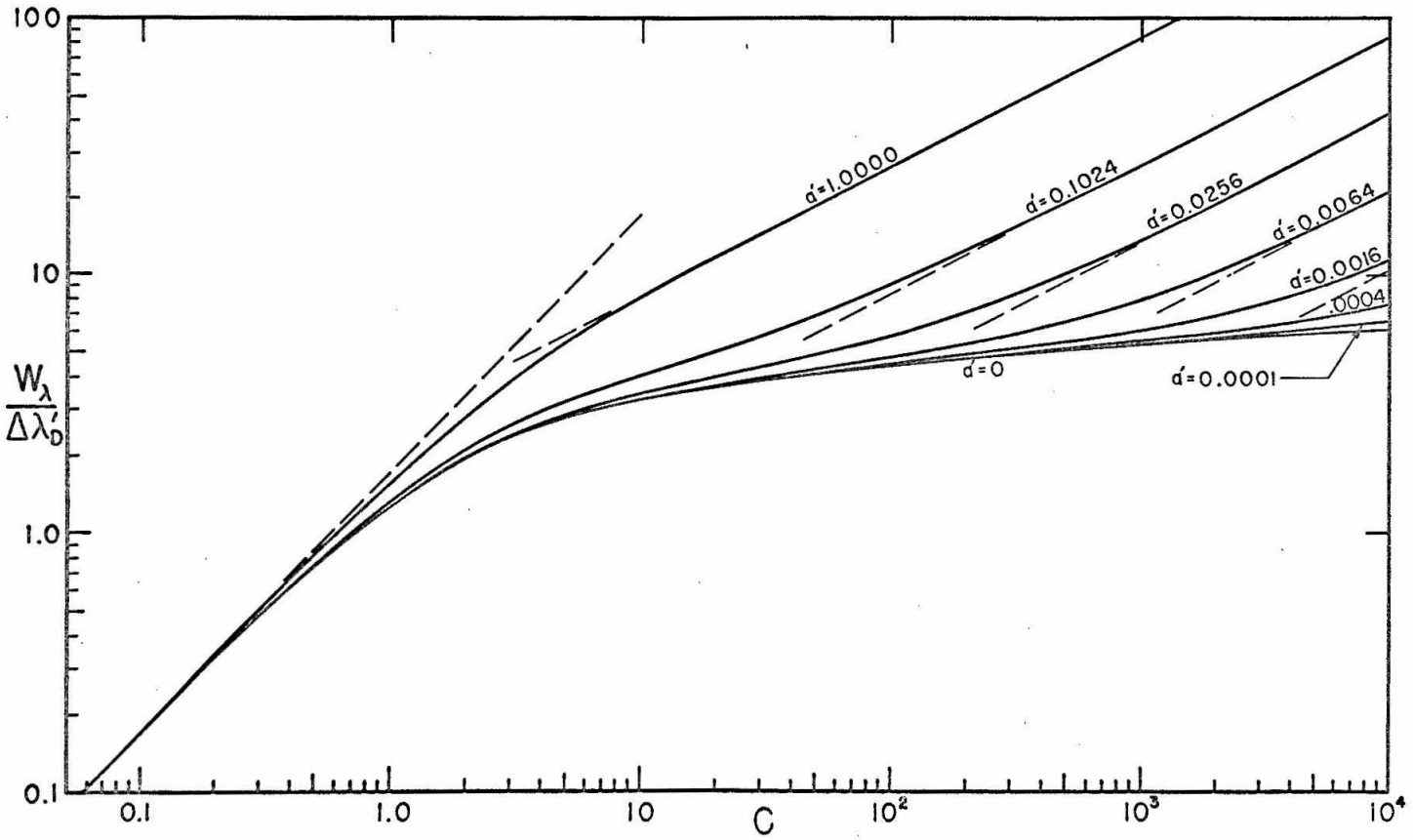

Figure 2. Theoretical curves of growth.

the fainter the line, the less accurately it can be measured. For these reasons most of the experimental data are taken on the upper end of the linear part, near the "knee" of the curve.

For most of the lines considered here the value of a' is less than 0.01, and in the region of interest the curves for $0 \leq a' \leq 0.01$ are virtually coincident so the curve of growth may be approximated by equation (32). However, for λ2288 of Cd, data can only be obtained above the linear part. This line also has a large value of a' so the curve of growth must be calculated using equation (22) (modified as described in Section II-F because of isotopic and hyperfine structure).

D. The Deposit Rate

The value of K is determined by weighing the atoms which go through a circular aperture of radius ρ at a height $z = b$ above the orifice as shown in Figure 1. The rate $\mathcal{N}_p$ at which atoms go through this aperture is obtained by integrating equation (1) over velocity and the solid angle Ω_p of the aperture measured from the orifice:

$$\mathcal{N}_p = \int_0^\infty dv \int_{\Omega_p} d\Omega \; \mathcal{N}_v(\theta)$$

$$= K \beta^3 \int_0^\infty v^3 \; e^{-\beta^2 v^2} \, dv \int_0^{\theta_p} \cos\theta \; 2\pi \sin\theta \, d\theta$$

$$= \frac{\pi}{2} \frac{K}{\beta} \sin^2 \theta_p$$

$$= \frac{\pi}{2}\frac{K}{\beta}\left(\frac{\rho^2}{b^2+\rho^2}\right) \quad . \tag{33}$$

When these atoms deposit on the microbalance pan the rate at which mass is added is

$$G = \frac{M}{N_o}\,\mathcal{n}_p = \frac{\pi\, K\, M}{2\,\beta\, N_o}\left(\frac{\rho^2}{b^2+\rho^2}\right) \tag{34}$$

where N_o is Avogadro's number.

Equations (2), (24), and (34) can now be combined and solved for the f-value:

$$f = \frac{Q\,T\,C}{G} \tag{35}$$

where

$$Q = \frac{2Rmc}{N_o e^2}\,\frac{z_o}{\lambda_o}\left(\frac{\rho^2}{b^2+\rho^2}\right) \tag{36}$$

and C is obtained from the measured value of W_λ and the appropriate curve of growth.

E. The Boltzmann Factor

For most of the elements studied with the atomic beam apparatus the excited states are sufficiently separated from the ground state so that, at the temperatures necessary to produce an atomic beam, essentially all the atoms are in the ground state and are capable of making the transition being studied. Some elements,

however, have several low-lying states which are appreciably populated at these temperatures, and in this case the deposit rate must be multiplied by the Boltzmann factor

$$F_B = \frac{g_\ell \, e^{-E_\ell/kT}}{\sum_i g_i \, e^{-E_i/kT}} \qquad (37)$$

where E_i is the energy of the i^{th} level and k the Boltzmann constant. In applying this factor it is assumed that the relative populations of the atoms in the atomic beam are the same as in the crucible. While the radiative lifetimes of these levels are long enough that they do not return to the ground state in the time it takes them to travel from the crucible to $z = z_o$, Lawrence[9] finds some evidence that levels with $E_i \gtrsim kT$ may be depopulated, perhaps by collisions in the atomic beam.

F. Hyperfine Structure and Isotope Shifts

Most of the lines studied have hyperfine and isotopic structure which is, at best, only partially resolved by the spectrograph. The theory which is derived for a single line in Sections B and C must be modified to take this into account. If the line consists of n components, of which the i^{th} component has fractional strength I_i and is centered at λ_i, then equation (22) generalizes to

$$\frac{W_\lambda}{\Delta\lambda_D'} = \int_{-\infty}^{+\infty} \left\{ 1 - e^{-C \sum_{i=1}^{n} I_i \, H(a', u-u_i)} \right\} du \qquad (38)$$

where

$$u_i = \frac{\lambda_i - \lambda_o}{\Delta\lambda_D'} \quad \text{and} \quad \sum_{i=1}^{n} I_i = 1 \ .$$

If the hyperfine and/or isotopic splittings are small compared to the Doppler width of the line, i.e. all $u_i \ll 1$, then they will have little effect and equation (22) can be used. On the other hand, if the splittings are all large, $(u_i - u_j) \gg 1$ for all pairs $i \neq j$, then each individual component does not overlap any other and each will follow its own curve of growth. The total curve of growth for the unresolved group is then

$$\frac{W_\lambda}{\Delta\lambda_D'} = \sum_{i=1}^{n} \int_{-\infty}^{+\infty} \left\{ 1 - e^{-C \, I_i \, H(a', u)} \right\} du \ . \qquad (39)$$

Thus, for any C, $W_\lambda/\Delta\lambda_D' = \sum_{i=1}^{n} (W_\lambda/\Delta\lambda_D')_i$ where $(W_\lambda/\Delta\lambda_D')_i$ is obtained from the single component curve of growth, equation (22), for $C_i = I_i \, C$. It is clear that the same procedure can be followed if the components occur in groups (as they often do) such that within each group the components have a spread which is small

compared to $\Delta\lambda_D'$, and each group is separated from the others by distances which are large compared with $\Delta\lambda_D'$. Qualitatively it can be said that if the total spread within each group is less than $1/2\ \Delta\lambda_D'$ and the centers of gravity of neighboring groups are separated by more than $3\ \Delta\lambda_D'$, then the curve of growth given by equation (39) can be relied on at least half way up the "knee."

If these conditions are not met, then either measurements must be made only on the linear part (which is fortunately extended by the splittings) or else the exact curve given by equation (38) must be calculated numerically.

G. Impulse Forces

When the shutter under the microbalance pan is opened, the pan experiences an upward force due to the momentum of the atoms in the atomic beam. Assuming all of the atoms stick to the pan, this force $\mathcal{F}$ is given by the rate of momentum transfer in the z-direction of the atoms impinging on the pan:

$$\mathcal{F} = \int_0^\infty dv \int_{\Omega_p} d\Omega \frac{M}{N_o} v \cos\theta \ \mathcal{N}_v(\theta)$$

$$= \frac{M}{N_o} K \beta^3 \int_0^\infty v^4 e^{-\beta^2 v^2} dv \int_0^{\theta_p} \cos^2\theta\ 2\pi \sin\theta\ d\theta$$

$$= \frac{\pi^{3/2}}{4} \frac{M}{N_o} \frac{K}{\beta^2} \left\{ 1 - \cos^3\theta_p \right\}$$

$$= \frac{\pi^{3/2} M K}{4 N_o \beta^2} \left\{ 1 - \left(\frac{b^2}{b^2 + \rho^2} \right)^{3/2} \right\} \quad . \qquad (40)$$

A more convenient quantity to measure is the ratio of the impulse force to the deposit rate. This quantity, known as the recovery time t_R because it is the time required for the micro-balance output to return to its value previous to opening the shutter, is given by

$$t_R = \frac{\mathcal{J}}{gG} = \frac{1}{g} \sqrt{\pi RT/2M} \left\{ \frac{b^2}{\rho^2} \left[\left(1 + \frac{\rho^2}{b^2} \right) - \left(1 + \frac{\rho^2}{b^2} \right)^{-1/2} \right] \right\} \qquad (41)$$

where g is the acceleration of gravity. These recovery times range between 0.5 and 2.0 minutes.

It is convenient to expand equation (41) in a power series in $(\rho/b)^2$:

$$t_R = \frac{3}{2g} \sqrt{\pi RT/2M} \left\{ 1 - \frac{1}{4} \left(\frac{\rho}{b}\right)^2 + \frac{5}{24} \left(\frac{\rho}{b}\right)^4 + \ldots \right\} \quad . \qquad (42)$$

In practice $(\rho/b) \lesssim 0.11$ so less than 0.3% error is made in using only the first term of the series.

H. Impulse Force Anomalies and Deposit Rate Corrections

There are several reasons why the experimentally measured recovery times may not agree with the theoretical values. If the

mechanism producing the discrepancy is known, an appropriate correction can be applied to the deposit rate. The possible mechanisms are: (1) Non-constant atomic beam flux, (2) The presence of molecules of the element being studied in the atomic beam, (3) Non-unity sticking coefficient of the atoms on the pan, and (4) Adsorption of residual gas by the metal deposited on the balance pan. These mechanisms are considered in detail in the Appendix. The results are that mechanism (1) can be recognized and the data discarded, and that (2) to (4) lead to correction factors of a similar nature which can be applied to the observed deposit rate.

Let the observed deposit rate be $(1 + \alpha)$ times the deposit rate which would have been obtained if all the desired atoms and no others stick to the pan. Then

$$\alpha = \frac{1 - (t_R^{obs}/t_R^{th})}{\Lambda + (t_R^{obs}/t_R^{th})} \tag{43}$$

where t_R^{obs} is the observed recovery time and t_R^{th} is the theoretical value given by equation (42). The constant Λ is given by

$$\Lambda = \begin{cases} -1/\sqrt{n} & \text{for n-atomic molecules in the atomic beam} \quad (44) \\ \frac{2}{3}\sqrt{T_p/T} & \text{for non-unity sticking coefficient} \quad (45) \\ \frac{2}{3}\sqrt{(T_p/T)(M/M_A)} & \text{for adsorption of residual gas} \quad (46) \end{cases}$$

where T_p is the temperature of the pan and M_A is the molecular weight of the adsorbed gas.

The observed deposit rate may be multiplied by

$$F_G = \left(\frac{1}{1+\alpha}\right) = 1 - \left(\frac{1}{1+\Lambda}\right)\left(1 - t_R^{obs}/t_R^{th}\right) \qquad (47)$$

to give the corrected deposit rate. As shown in the Appendix, the value of $1/(1+\Lambda)$ is approximately 0.5 to 0.8 but can rise to 3.414 if diatomic molecules are present in the beam. Even in the absence of any knowledge of the mechanism, an average value of 0.6 to 0.7 should give corrections which are good to 10% and if the corrections are no larger than 10% then the corrected deposit rates should be good to 1%. This assumes that the anomaly is not due to molecules, in which case the correction would be much too small. Even if molecules are suspected, the use of the corresponding value of $1/(1+\Lambda)$ is very risky because small errors in t_R^{obs} due to other mechanisms or instrumental errors would be greatly magnified.

I. Summary

In order to measure an f-value, the following quantities must be measured: equivalent width W_λ (mÅ), deposit rate G (μg/min), crucible temperature T (°K), and various geometrical factors z_o, b, ρ (inches), and sin θ. In addition the wavelength λ_o (Å) of the line, any hyperfine and/or isotopic structure, and the atomic weight (g/mole) of the element are needed.

The numerical factors in the following equations are appropriate for the units given in parentheses. Using equation (23) the Doppler width $\Delta\lambda_D'$ (mÅ) is calculated:

$$\Delta\lambda_D' = \frac{\lambda_o}{c}\sqrt{2RT/M}\ \sin\theta_o = 4.3021 \times 10^{-4}\ \lambda_o \sin\theta_o \sqrt{T/M}\ . \quad (48)$$

A value for f is estimated and the value of a' is calculated from equation (29):

$$a' = \frac{2\pi e^2}{m c^2 \Delta\lambda_D'}\ \frac{g_\ell}{g_u}\ f = 0.17705\ \frac{g_\ell}{g_u}\ \frac{f}{\Delta\lambda_D'}\ . \quad (49)$$

Then C is obtained from the appropriate curve of growth, equation (22), (32), (38), or (39). Finally, the f-value is calculated from

$$f = \frac{Q\ T\ C}{F_B\ F_G\ G} \quad (50)$$

where Q is given by

$$Q = \frac{2\ R\ m\ c}{N_o\ e^2}\ \frac{z_o}{\lambda_o}\ \left(\frac{\rho^2}{b^2+\rho^2}\right) = 498.10\ \frac{z_o}{\lambda_o}\ \left(\frac{\rho^2}{b^2+\rho^2}\right). \quad (51)$$

Either F_B or F_G or both may be unity.

In principle it would be necessary to put the resulting f-value back into a', and then iterate to obtain a consistent result. However, in practice, this is not necessary since the region of the knee of the curve of growth on which the data usually falls is quite insensitive to the value of a'.

III APPARATUS

A. Vacuum System

The vacuum chamber and atomic beam furnace have been described by Davis.[4] The furnace is enclosed in an 8 1/2 inch diameter brass cylinder 10 inches high with quartz windows sealed to two side arms which let the light beam through. A 1/2 inch thick brass base plate contains electrical and water cooling feedthroughs for the furnace. The microbalance is mounted on a 1/2 inch thick aluminum alloy plate which rests on top of the brass cylinder and is covered with a glass bell jar. There are approximately thirty demountable seals using viton O-rings.

The vacuum is produced and maintained by a Kinney 4 inch diffusion pump with a 5 cu ft/min Kinney forepump. Dow Corning DC-705 silicone pump oil is used in the diffusion pump. There is a liquid nitrogen cold trap in a water cooled baffle above the diffusion pump. The ultimate pressure which can be attained is slightly below 10^{-7} torr as measured with a Veeco RG 75K ionization guage. However, the pressure is usually at least ten times higher while data are being taken because of outgassing caused by the hot furnace.

B. Atomic Beam Furnace

The element to be vaporized is placed in a cylindrical crucible of graphite or zirconia and heated in a furnace tube of graphite or tantalum respectively. A small orifice in the side of the

crucible forms the source of the atomic beam. The furnace tubes must have a larger hole in them to provide clearance for the beam. Details of the crucibles and furnace tubes are given by J. K. Link.[10]

The ends of the furnace tube are clamped in water-cooled copper blocks and the furnace is heated by up to 300 amperes of alternating current. Power for the furnace is provided from a 115 v line by a 3 kv Sola constant-voltage transformer, and the furnace power is controlled by a 40 amp Variac. The constant-voltage transformer makes the furnace power regulator, which was formerly used by Davis[4] and Bell,[5] unnecessary. Temperatures in the crucible of over 2000° C can be produced if the furnace tube is surrounded by a radiation shield.

The furnace is surrounded by a water jacket with a slot in it which defines the solid angle of the atomic beam. A water-cooled plate with the circular aperture, which determines the portion of the atomic beam which goes to the microbalance pan, is mounted 7 inches above the furnace. Between this plate and the pan there is a shutter which is operated manually from outside the vacuum chamber.

A window is provided in the vacuum chamber for sighting into the orifice of the crucible with an optical pyrometer to measure the temperature. Because the atomic beam deposits would otherwise darken it, a disk of glass is installed under the window which can be rotated from outside the vacuum chamber to provide a clean surface for each temperature measurement. Besides the window and disk, there is a right angle prism outside the chamber to obtain a more convenient viewing angle. These components reduce the amount of radiation reaching

the pyrometer so a correction curve was obtained by measuring the temperature of a tungsten ribbon lamp with and without the windows and prism. The corrections range from 15° C at 800° C to 69° C at 2100° C.

Cadmium vaporizes at temperatures which are much too low to measure with an optical pyrometer, so a special graphite curcible was constructed with a platinum to platinum - 10% rhodium thermocouple in it. The thermocouple was contained in an alundum thermocouple tube with the end cemented over with Saueriesen #7 cement. This tube protruded through one end of the crucible with the thermocouple junction under the orifice and was cemented in place with Sauereisen.

The thermocouple was compared with the optical pyrometer at temperatures between 800° C and 1500° C and found to read 12° C to 40° C low with the largest difference at low temperatures. A rough theory considering heat conduction along the thermocouple tube and radiation from the walls of the crucible to it accounted for these differences if the heat conductivity of the alundum tube was properly chosen. At low temperatures the difference should rise linearly with the difference from room temperature; the difference reaches a maximum and then falls at high temperatures because of the increased transfer of heat to the tube by radiation from the crucible.

In practice, the freezing temperature of cadmium (320.9° C) was observed by the step on a cooling curve and the corrections were assumed to be linear with the difference between room temperature and the crucible temperature. While the correction varied between 11° C and 35° C at T = 321° C for various runs, it remained quite constant

during any one run.

C. Microbalance

The microbalance was originally built by G. M. Lawrence[9] with the electronics designed and built by the present author. Since the work of Lawrence, Link, and King,[11] the electronics have been rebuilt to provide about a factor of ten reduction in noise. In addition, most parts of the microbalance itself have been replaced because of breakage.

Figure 3 shows the structure of the microbalance. It uses the magnet structure and torque coil of a small 0-500 μA panel meter. The pivots have been replaced with a taut band suspension system in which the springs, which originally provided the restoring torque for the meter, have been stretched out and soldered to the tips of the original pivots to form the taut bands. A small spring provides tension.

The pointer has been replaced with a beam made from a drawn out glass tube about 0.030 inch in diameter and 5 3/4 inches long, which is cemented to the coil at one of the pivots with polystyrene cement. The pan is suspended from one end of the beam 3 1/4 inches from the torque coil. Three counterweights made of different sizes of copper wire can be slid along the other end to adjust the static balance.

Pans weighing about 30 mg are made from 0.25 mil thick aluminum foil. A quarter sector of a 1.8 inch radius circle of foil is

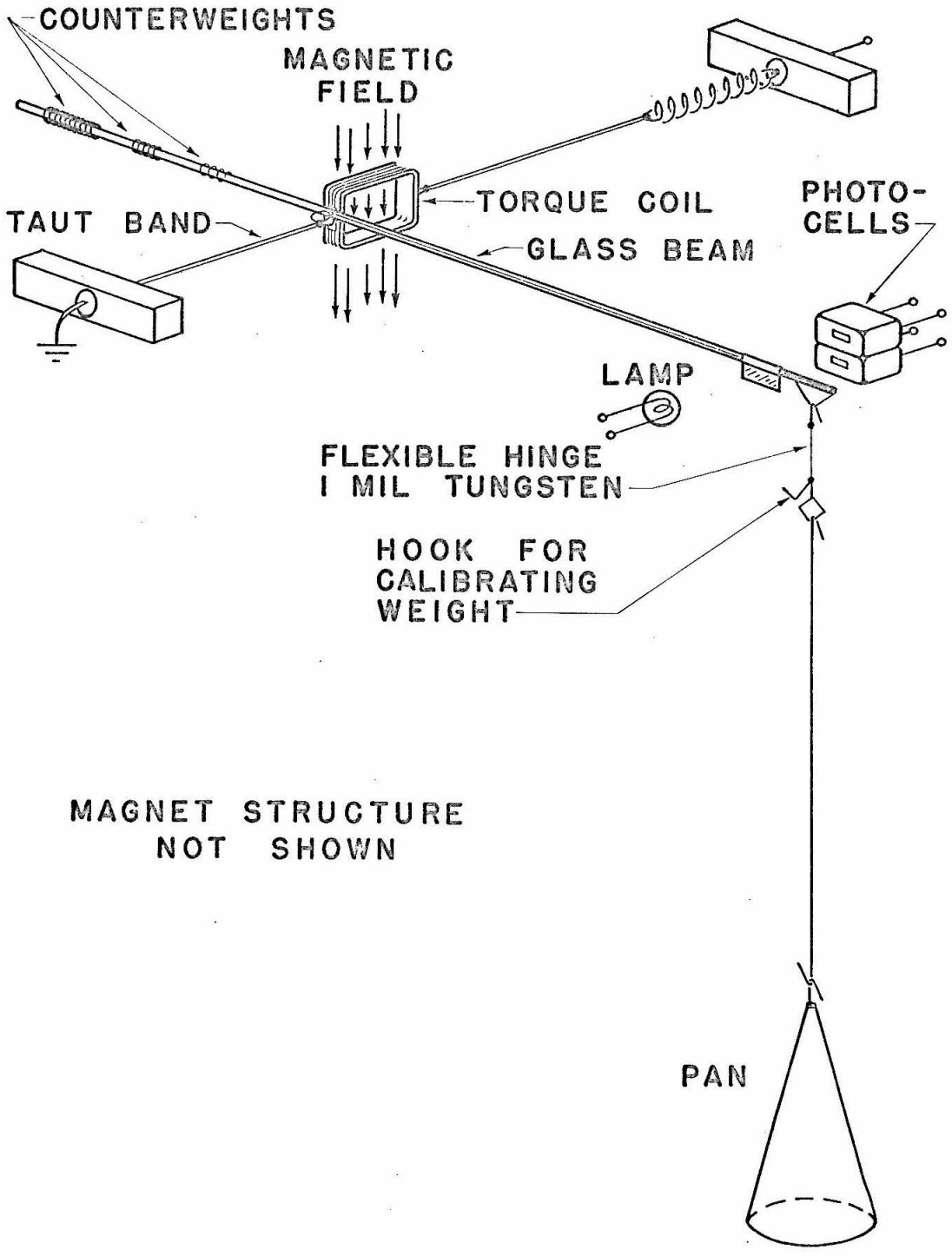

Figure 3. Microbalance construction.

formed into a cone with a 1/16 inch wide folded seam. Approximately 1/16 inch of the open end is folded inward providing a more rigid structure, and a small hook of 5 mil diameter aluminum wire is attached to the apex. The pans are made conical to increase the fraction of the incident atoms which stick; any atom which does not stick on the first encounter has a good chance of hitting the pan again.

A 5 mil nichrome wire passes through the microbalance beam from the torque coil to the end where it is formed into a stirrup. This grounds the pan, removing the possibility that it might become electrically charged. Such a charge, if it raised the pan to a potential of 100 volts, would result in spurious forces of approximately 12 μg as the shutter was operated.

J. K. Link[10] found that placing a light bulb near the pan partially prevented the adsorption of residual gases by the fresh deposit. In the present experiment this function is provided by several turns of nichrome wire which surround the pan and may be heated red hot. The use of the pan heater is described in Sections IV-B, C.

A permanent magnet is placed near the pan to damp out pendulum oscillations by means of induced eddy currents. The magnet could not be used for atomic beams of iron so the flexible "hinge" shown in Figure 3 was replaced by a rigid support wire and damping was supplied by sliding friction at the stirrup. This method of suspension leads to greater noise in the output signal due to changes in the exact position of the suspension wire in the stirrup.

The microbalance is balanced by adjusting the current through the torque coil until it is at rest at a given position so that changes in the current are accurately proportional to changes in the mass of the pan despite any variation of the strength of the magnetic field with angle. A feedback system keeps the microbalance continuously balanced. The position of the beam is sensed by two RCA 6694-A cadmium sulfide photocells illuminated by a number 222 prefocused flashlight bulb. A flag on the beam covers one photocell and uncovers the other as the beam moves. The output of this detector is amplified by a two-stage complementary transistor amplifier as shown in Figure 4, and the output is fed back to the torque coil through resistor R_o and capacitor C_o. The capacitor provides feedback proportional to the velocity of the beam and is chosen to produce nearly critical damping. The feedback gain is greater than 1000 and produces a restoring torque much greater than that of the taut band suspension system. In fact the microbalance itself is mechanically unstable because the beam is cemented above the taut bands, and thus it cannot be balanced without the automatic feedback system.

In addition to the current produced by the amplifier, current in the torque coil can be varied manually through resistors R_1 and R_2. In use the manual balance controls are adjusted so that the amplifier output is near zero. The amplifier can supply a current equivalent to $\pm$ 2.2 mg and the manual controls $\pm$ 5.5 mg.

The output of the amplifier is filtered by capacitors C_1 and C_2 and fed through the range switch into a Moseley Autograf Model 680

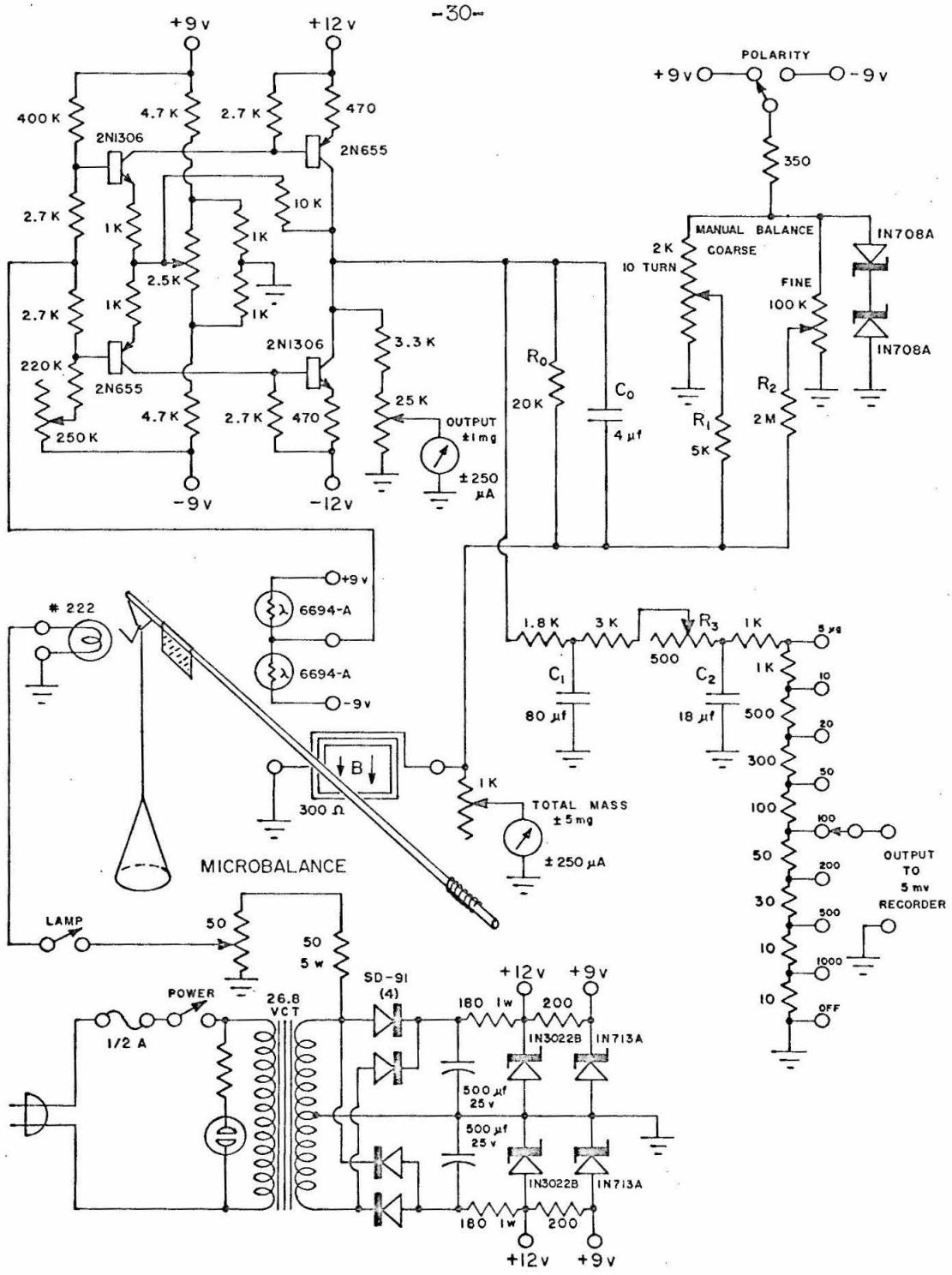

Figure 4. Microbalance circuit.

chart recorder. The following ranges are provided: 5, 10, 20, 50, 100, 200, 500, and 1000 μg full scale.

The power supply for the microbalance electronics is well stabilized by Zener diodes. The power to the manual balance controls must be especially well regulated as can be seen from the following consideration. When these controls are providing a current to the coil equivalent to 5 mg, a shift in that current of only 0.01% will cause a shift in the output of 0.5 μg.

The microbalance is calibrated by hanging a 1 mg class M weight from a hook on the pan suspension and adjusting the calibration control R_3 until the weight produces full scale deflection of the recorder on the 1000 μg scale. A manipulator allows this to be done while the vacuum system is pumped down.

Fluctuations in the microbalance output amount to 0.04 μg peak-to-peak and drift is less than 0.005 μg/min when the equipment is thoroughly warmed up. The response to a sudden change in mass shows a rise time of 0.0035 to 0.005 minutes (0.2 to 0.3 sec.) depending on the amplitude on the chart recorder. This is small enough so that it does not affect the measurement of recovery times.

Tracings of two microbalance recordings are shown in Figure 5. The first shows the data for some of the smallest deposit rates recorded. The second is typical of data that can be obtained for deposit rates of 4 μg/min or greater. Such recordings often do not deviate from a straight line by more than the width of the ink line.

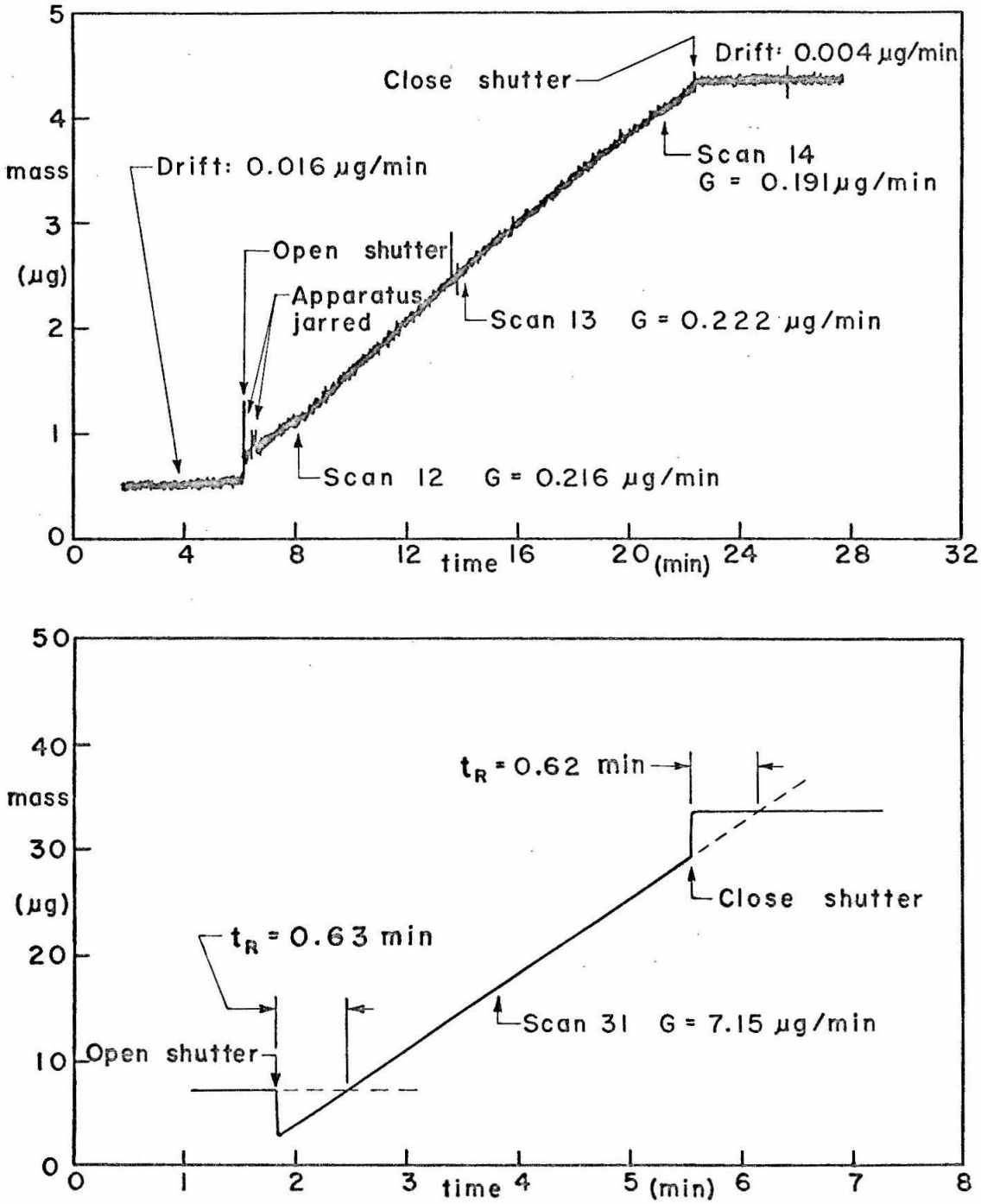

Figure 5. Microbalance recordings. From cadmium run, July 19, 1966.

D. Optical System

Figure 6 is a diagram of the optical system. Light from the horizontally mounted capillary tube of the lamp is imaged in the atomic beam by lens #1 (approximately 15 cm focal length) and reimaged on the spectrograph slit by lens #2 (25 cm). These lenses are made of quartz and are not achromatic so the optical system must be refocused for each wavelength. This is accomplished by adjusting the positions of the lamp and lens #2. The stop is a 1/4 inch diameter aperture placed around the virtual image of the spectrograph grating to eliminate extraneous light. The light modulator varies the amount of light reaching the spectrograph in such a way as to remove fluctuations in the intensity of the lamp.

In developing the theory, it was assumed that the transverse dimensions of the light beam are negligible as it passes through the atomic beam. This, of course, refers only to that part of the beam which is subtended by the grating and is diffracted to the phototube. The thickness of this beam varies from 0.08 mm directly over the orifice to 1.0 mm as it enters and leaves the atomic beam. The horizontal width is 7.2 mm. Compared with the height above the orifice (z_o) of 2.5 cm, these dimensions are small enough that less than 1% error is made by the assumption that the transverse dimensions of the light beam are negligible.

The light source is a PEK Labs type A high pressure mercury arc lamp operated at 500 to 1500 v dc from a motor-generator set. It draws a current of about 1 amp. The discharge is contained in a 3 cm

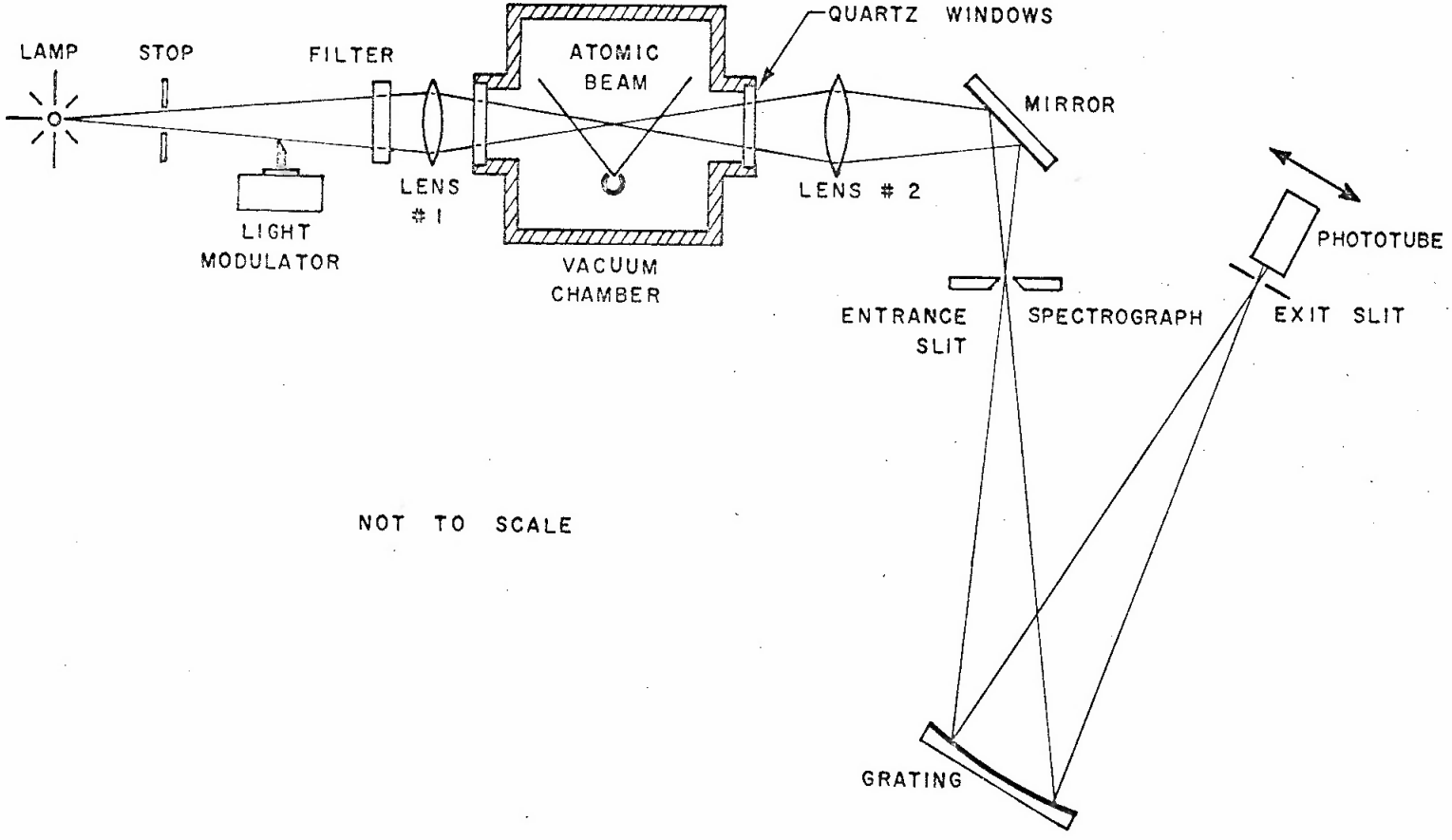

Figure 6. Optical system.

length of 1 mm bore quartz capillary tube, which is surrounded by a quartz water jacket. The lamp is cooled with tap water, which slowly deposits salts on the capillary tube and water jacket resulting in a gradual decrease in the intensity, especially at very short wavelengths. These deposits may be removed with dilute hydrochloric acid.

Figure 7 shows the spectrum which is produced by the lamp in this optical system. It is similar to the spectrum obtained by Stahl[16] and consists of pressure-broadened emission lines with strong continuum radiation between them. The drop-off in intensity at the extremes of the spectrum is due partly to the blaze of the spectrograph grating. It is of interest that in regions near emission lines or below 2500 Å the intensity decreases with increasing power to the lamp. All data reported here were obtained in wavelength regions far removed from any of the emission lines.

The filter shown in Figure 6 is used to limit the light reaching the spectrograph to that in the desired order. For wavelengths between 3500 Å and 3900 Å a Corning glass filter no. 7-59 "Blue Purple Ultra" is used. Between 2800 Å and 3500 Å the filter is no. 7-54 "Red Purple Corex A." Below 2800 Å a liquid filter is used, which consists of a solution of 180 g $NiSO_4 \cdot 6H_2O$ plus 80 g $CoSO_4 \cdot 7H_2O$ per liter of water contained in a quartz cell with a thickness of 3.5 cm. This filter is a compromise between those recommended by Strong[17] p. 363 and Krasha.[18] It passes light between 2200 Å and 3400 Å. To prevent excessive absorption below 2500 Å, it must be made with extremely pure water.

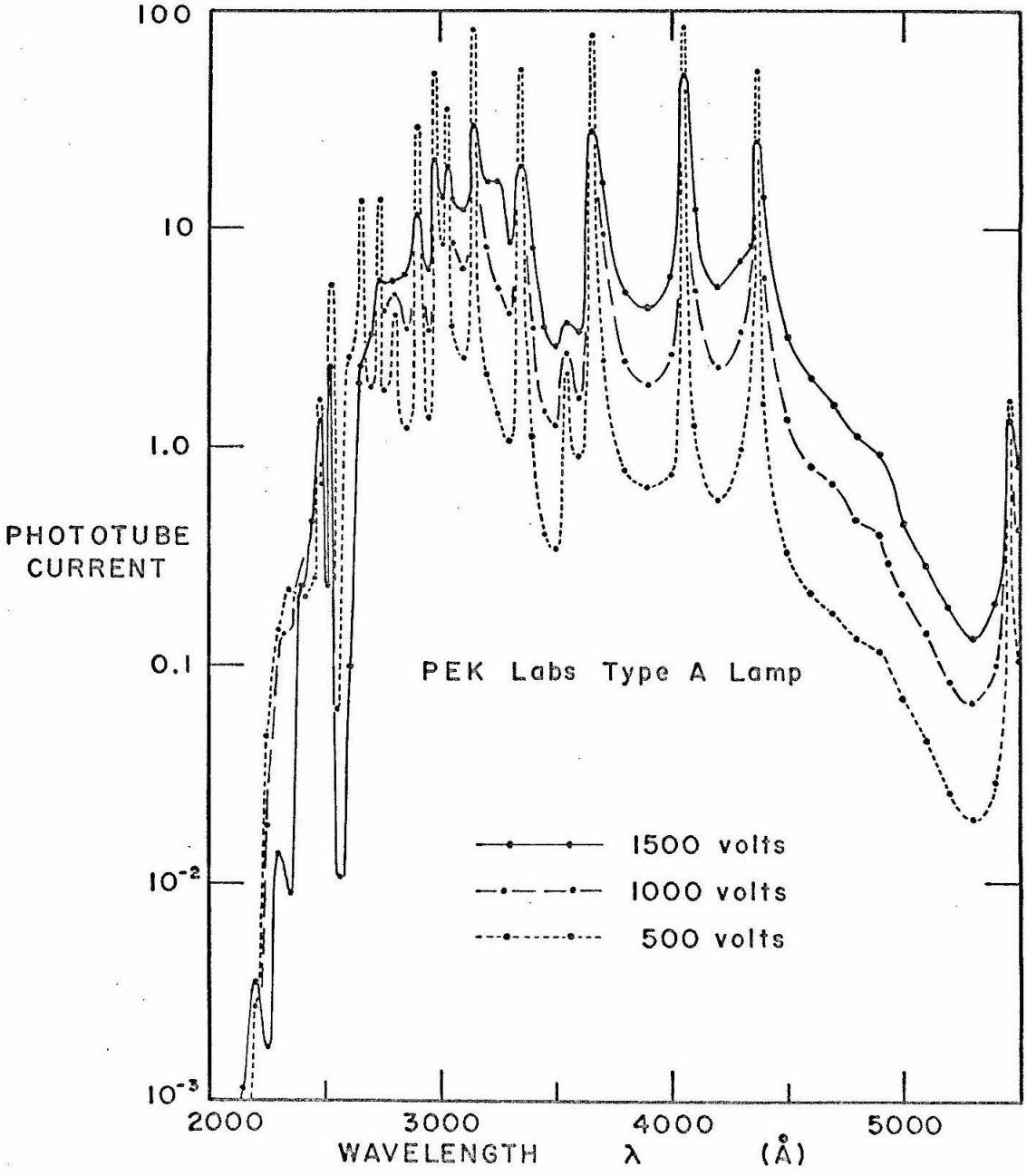

Figure 7. Lamp spectrum.

The light transmitted through the atomic beam is analyzed by a 21 foot Rowland spectrograph. The Bausch and Lomb grating has a radius of curvature of 6.65 meters and a ruled area 13.8 cm long with 600 rulings per mm. It is used in second order where the dispersion is 1.253 Å/mm. The entrance slit was set at 15 to 40 microns with an exit slit of 21 microns. Figure 13b gives an indication of the resolution which can be obtained. The hyperfine components of the copper line λ3247, which are about 40 mÅ apart (see Section IV B), are partially resolved. Theoretically the resolution of the grating at this wavelength is 20 mÅ, but this is degraded to more than 35 mÅ because of the finite widths of the slits.

The amount of scattered light in the spectrograph has been estimated by inserting filters in the light path which cut out the wavelength for which the spectrograph is focused and pass large bands of the spectrum at other wavelengths. At wavelengths above 2500 Å these measurements indicate that the amount of scattered light is negligible. However, below 2500 Å, where the light intensity is small compared to the intensity at longer wavelengths, significant amounts of scattered light are present and must be taken into account. As described in Section IV-C, 12.6% of the photocurrent at 2288 Å was found to be due to scattered light.

At the camera holder of the spectrograph there is a carriage containing the exit slit and photomultiplier tube detector which are scanned along the focal curve to record the spectrum. In addition, there is a reference photomultiplier tube and an associated system of

mirrors which supplies a signal to the light regulator system. This carriage replaced a similar one used by Lawrence and Link,[9,10,11] in which a reference signal was obtained through a light chopping arrangement.

The exit slit was constructed from razor blades in the manner described by Lawrence,[9] p. 34. In keeping with advances in the state of the art, Wilkinson Sword stainless steel blades were used instead of the Gillette Super Blue Blades previously used. The width of the slit varies from 20 to 23 microns over a length of 2 cm with an effective average being 21 microns.

The light passing through the exit slit is detected by an EMI/US type 9526B photomultiplier tube which has a quartz end window. Its response extends from below 2000 Å to above 6000 Å. The dark current is less than one nanoampere, which is negligible compared to the signal current which is usually between one and three microamperes.

Power for the photomultiplier tube is obtained from a John Fluke model 402M high voltage power supply which is regulated to 0.01%. Typically, the voltage was set at 1200 to 1300 volts except for wavelengths below 2500 Å where voltages up to 1600 volts were used because of the small amount of light available.

The carriage is driven up and down the focal curve of the spectrograph by a Starret no. T465P micrometer head. Power is supplied by an Apcor model 2201-60 multiratio gearmotor coupled to a thirty-to-one worm reduction gear. Except for the multispeed gearmotor, this driver is identical to that described by Lawrence,[9] p. 30. The

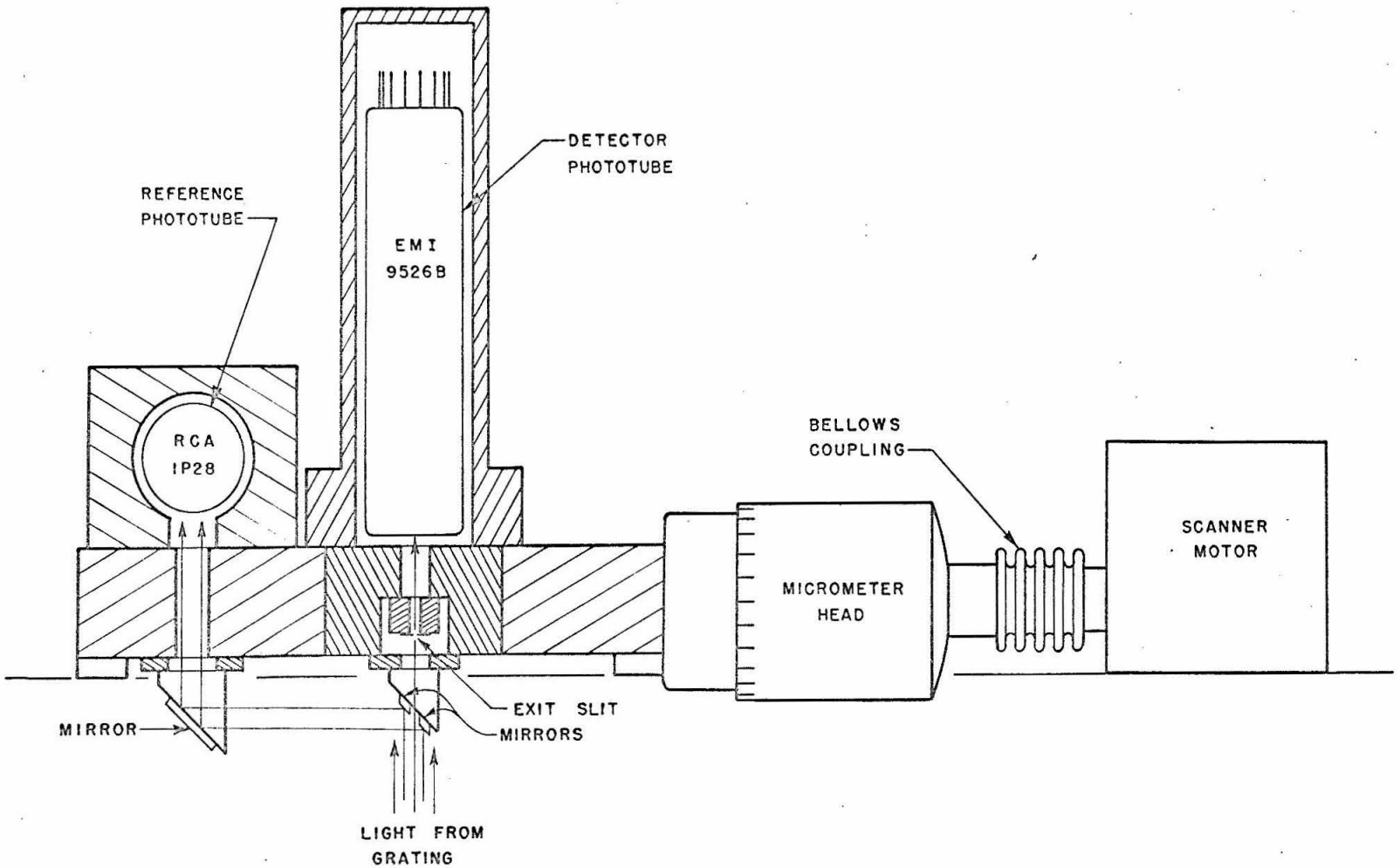

Figure 8. Carriage.

scanning speeds which are available are: 1, 2.5, 5, 10, 25, and 50 mils per minute. Most of the data was taken with a scanning speed of 2.5 mil/min although 5 and 10 mil/min were also used. The faster speeds are useful for finding lines.

Since the widths of the absorption lines are only about 2 to 3 mils at the focal curve of the spectrograph, the motion of the carriage must be very precise. Although the carriage is driven by a synchronous motor so that its average speed is constant, there occasionally appears to be short-term variations in the scanning velocity. This is indicated by comparing average f-values obtained while scanning in the two directions; if the difference is greater than the scatter in the individual values, velocity variations are suspected. Attempts to measure the instantaneous velocity of the carriage have been only partly successful due to its extremely small value. However, at one time an increase in velocity of approximately 13% for one-half minute was observed along with several smaller increases and decreases. These variations were observed while scanning in one direction but not the other. Most of the time, the scanning velocity seemed to be constant to within 2% when averaged over 10 seconds. Disturbances such as these are minimized by carefully polishing the track in which the carriage slides with #600 emery paper and lubricating it with "Lubriplate."

E. Light Regulator

Because the light intensity at different wavelengths is

measured at different times as the carriage is driven across the spectrum, it is important that the intensity of the continuum be constant with time. Unfortunately the light output of the lamp fluctuates. These fluctuations consist of continual variations of about 1%, sudden jumps in the intensity of about 10%, which occasionally occur as often as every minute or so (or occasionally not at all), and a long term decrease of up to 10% per hour due mostly to the deposition of cooling water contaminants on the lamp and water jacket. The purpose of the light regulator is to remove these fluctuations.

The light regulator operates by forcing the output of the reference photomultiplier tube to remain constant. It does this by varying the fraction of the lamp's output which reaches the spectrograph through the action of the light modulator and also by varying the power to the lamp.

As shown in Figure 8, the 1P28 reference photomultiplier tube is mounted on the carriage and, by means of mirrors, looks at two bands of the spectrum which straddle the portion seen by the detector photomultiplier tube. Experience has shown that fluctuations in the lamp output at different wavelengths are poorly correlated if the wavelengths are not close together. Therefore, the two bands seen by the reference tube are made small and close together. Figure 9 shows the response of the reference system in relation to the detector wavelength as measured by scanning a monochromatic source and recording the sum of both phototube signals.

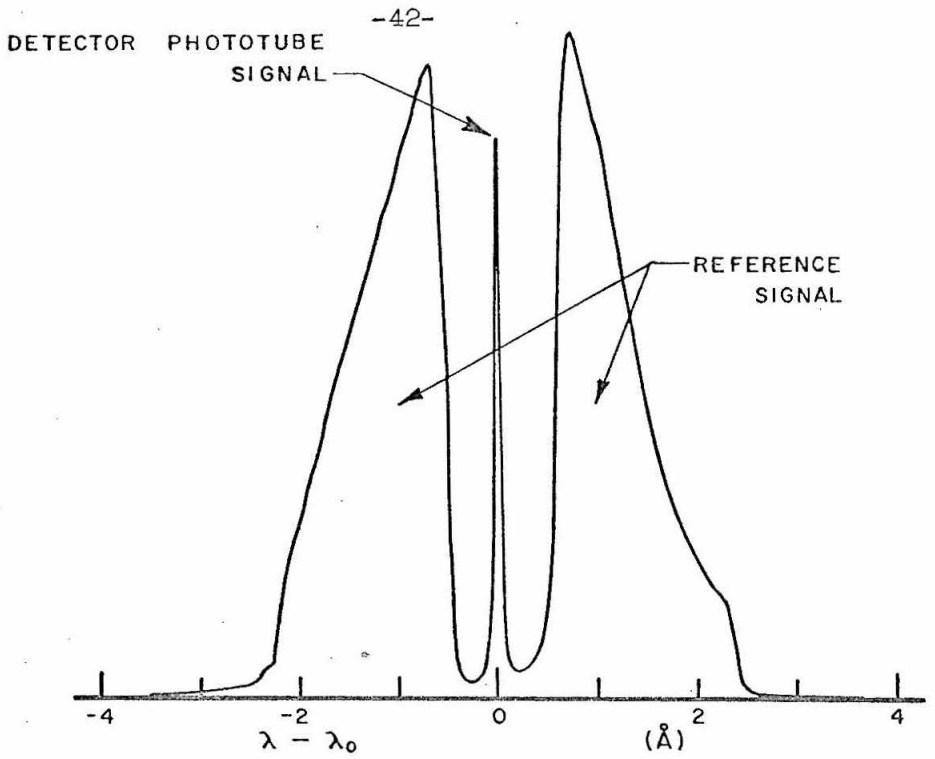

Figure 9. Relative response of reference photomultiplier tube.

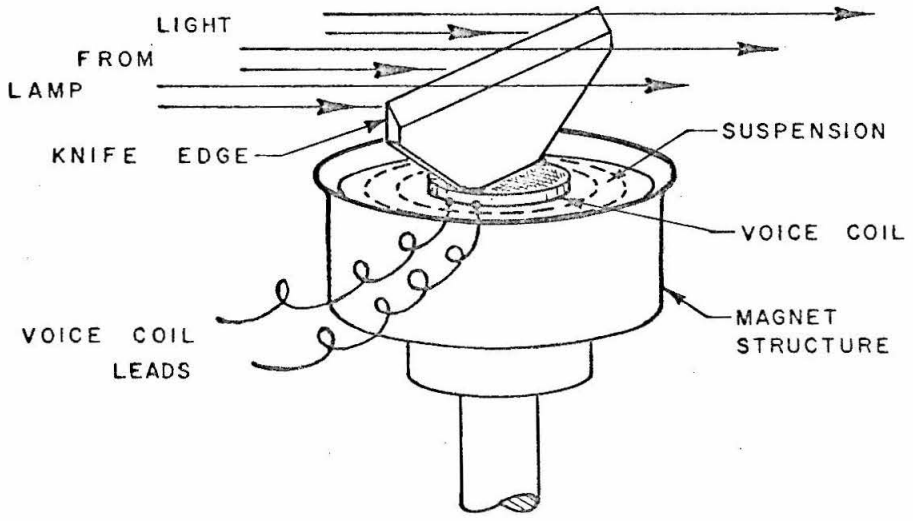

Figure 10. Light Modulator.

The entire reference signal comes from wavelengths within $\pm$ 2 1/2 Å of the wavelength seen by the detector tube.

The light modulator was constructed from a small loudspeaker as shown in Figure 10. The cone and excess sheet metal were removed and a bakelite knife edge was cemented to the voice coil. Its resonant frequency is 100 cycles per second with a damping ratio of 0.45. It is placed in the light beam between the stop and the filter as shown in Figure 6 and is positioned so that it blocks out approximately 25% of the light to the spectrograph. As signals are applied to it, the voice coil moves up or down blocking out more or less light.

The circuit diagram of the light regulator is shown in Figure 11. Voltage for the reference photomultiplier tube is obtained from the same power supply that powers the detector tube but can be varied from 40 to 100% of that voltage by R_1. This controls the gain of the phototube, which is always operated with a photocurrent of 20 μA regardless of the light level.

The current from the reference tube is filtered by R_2, R_3, and C_1 to reduce the high frequency response so that the amplifiers are not overloaded by noise due to statistical variations in the rate at which photons reach the phototube. A constant current of 20 μA is subtracted from the photocurrent through R_4 and the difference is amplified by a preamplifier consisting of transistors Q_1 through Q_6 and their associated components. The gain of this preamplifier can be varied by nearly 40 db by a feedback gain control. The three small

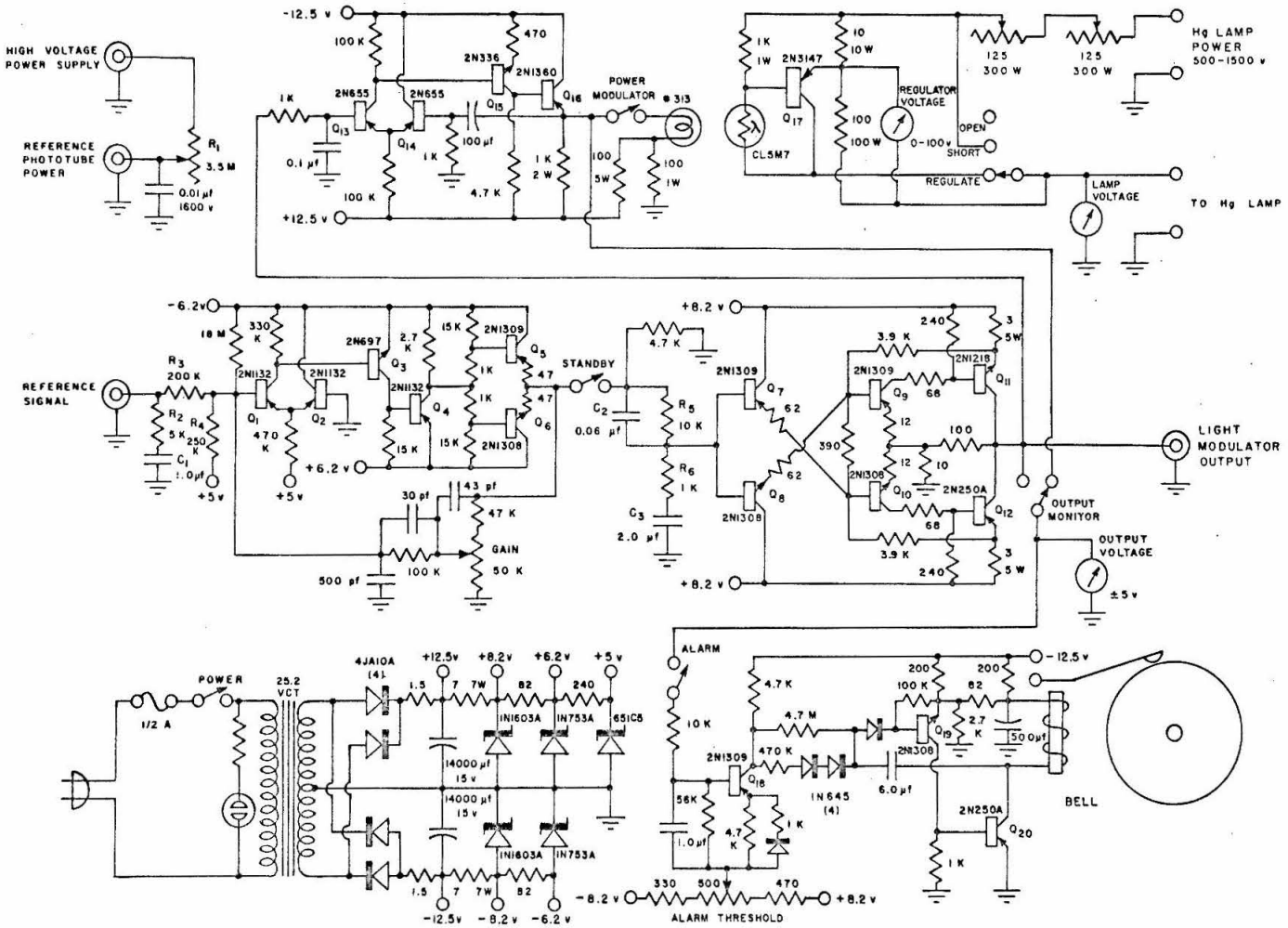

Figure 11. Light regulator circuit.

capacitors associated with the gain control are necessary to eliminate high frequency instabilities.

The output of the preamplifier is applied to a compensation network consisting of R_5, C_2, R_6, and C_3. This is a "lead-lag" network which adjusts the frequency and phase response of the overall feedback loop so that it is stable. The component values were chosen by the use of root-locus plots.

The light modulator is driven by a complementary amplifier with transistors Q_7 through Q_{12}. This amplifier has a high input impedance so that it does not load the compensation network and has an output voltage swing of ± 5 volts into the 6 ohm impedance of the light modulator.

After operating the light regulator with these components, it was noticed that, although the total gain is more than 60 db, changes in the light intensity due to changes in the lamp power were not completely removed. This suggested that additional improvement could be obtained by modulating the power to the lamp.

The lamp power is modulated by transistor Q_{17}, which is controlled by a cadmium sulfide photocell illuminated by a small lamp. In this manner signals are transmitted to Q_{17} despite the 500 to 1500 volt potential between it and ground. In consideration of the maximum voltage and power ratings of Q_{17}, the range over which it can vary the mercury lamp voltage is limited to about 100 volts. In practice, this has usually been sufficient although there have been times when a larger range would have been useful.

The #313 lamp is driven by Q_{13} through Q_{16} which amplify the voltage applied to the light modulator. Thus, the lamp power modulator circuit forces the light intensity to be such that no action is needed by the light modulator.

It would seem much simpler to eliminate the light modulator and modulate the lamp power directly with the signal from the reference phototube, but all attempts to do this have failed. The difficulty lies in the impedance and transfer functions of the lamp. These characteristics are non linear, often negative, and vary with time. When inserted in a feedback loop they almost invariably result in instabilities and oscillation. Such difficulties are largely circumvented by severely limiting the frequency response of the power modulator circuit so that only the DC characteristics are involved. Even so, the power modulator cannot be used at those wavelengths and lamp voltages where the light output remains constant or decreases with increasing lamp power. In normal operation the light modulator removes the fast fluctuations in the light intensity while the lamp power modulator takes over at very low frequencies and DC.

An alarm circuit is provided, consisting of transistors Q_{18}, Q_{19}, Q_{20}, and a modified doorbell. It may be operated from either the light modulator or power modulator outputs. Whenever the chosen output becomes more negative than a preset threshold, indicating that the lamp voltage needs to be increased manually, the bell rings, slowly at first and then more rapidly as the situation becomes more urgent. Thus, the operator can divert his attention from the light regulator

and still be informed when the lamp characteristics change. The circuit would be more useful if it also included an upper threshold as the lamp output occasionally increases with time.

The performance of the light regulator system is indicated by the size of the noise and drift of the continuum as displayed in Figure 13a. At wavelengths where the light intensity is large, the noise is usually less than 0.1% peak-to-peak with the signal filtered by two low-pass filters of 5 or 10 second time constants. This noise is due almost entirely to photoelectron statistics and can therefore not be reduced unless the light intensity is increased.

F. Equivalent Width Recording

The signal from the detector photomultiplier tube is processed as shown in Figure 12. After passing through a low-pass filter consisting of R_1 and C_1, it is amplified and filtered again by a chopper stabilized DC operational amplifier. The signal is then displayed on a Brown chart recorder either directly or with a constant DC voltage subtracted from it so that small changes may be observed.

The time constants $\tau_1 = R_1 C_1$ and $\tau_2 = R_2 C_2$ of the two low-pass filters are usually set at 5 or 10 seconds which, at the scanning speed of 79.6 mÅ/min, provides the most noise filtration without excessively smearing out the absorption lines being measured. For strong lines where the signal-to-noise ratio is larger, smaller time constants are sometimes used.

Range switches for the two outputs are set so that both

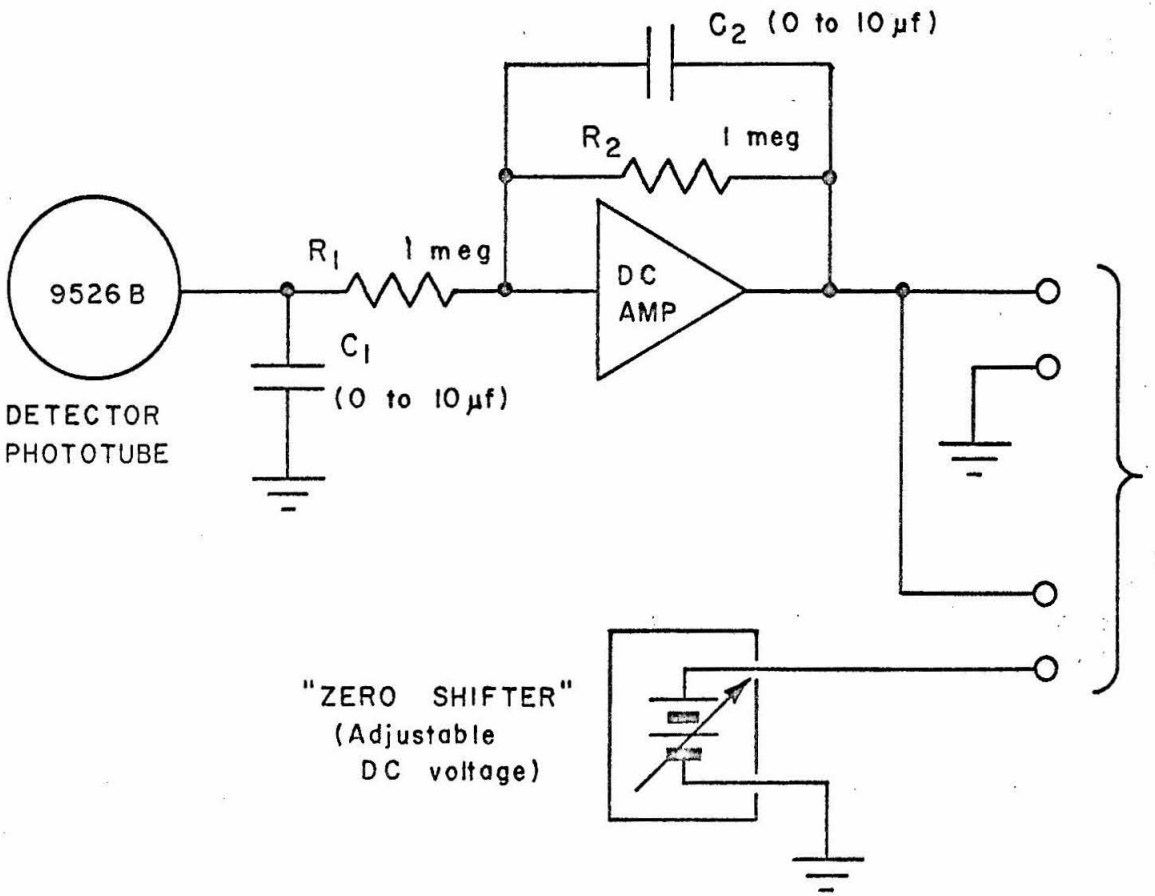

Figure 12. Photocurrent amplifier.

signals cover a large span on the chart recorder with the zero shifted signal displayed at a magnification of up to 100 times compared to the unshifted signal. This magnification is known as the scale ratio. While scanning a line the magnified signal is normally recorded. To record the continuum level, the recorder is switched to the unshifted signal for a few seconds. This may be done automatically either at one minute intervals or whenever the scanning direction is reversed.

Figure 13 shows two examples of the recorded data. To obtain the equivalent width a straight line is drawn connecting the continuum on each side of the line and the area is measured with a planimeter. The equivalent width is proportional to the area divided by the continuum level and scale ratio.

The smallest equivalent widths which can be measured with this apparatus are about 0.1 mÅ. This is 2 to 3 times better than the performance of the light chopping apparatus used by Lawrence and Link. The improvement is due to the elimination of noise from irregularities in the chopping process, better photoelectron statistics, and the fact that the reference signal is taken closer to the wavelength being observed by the detector tube.

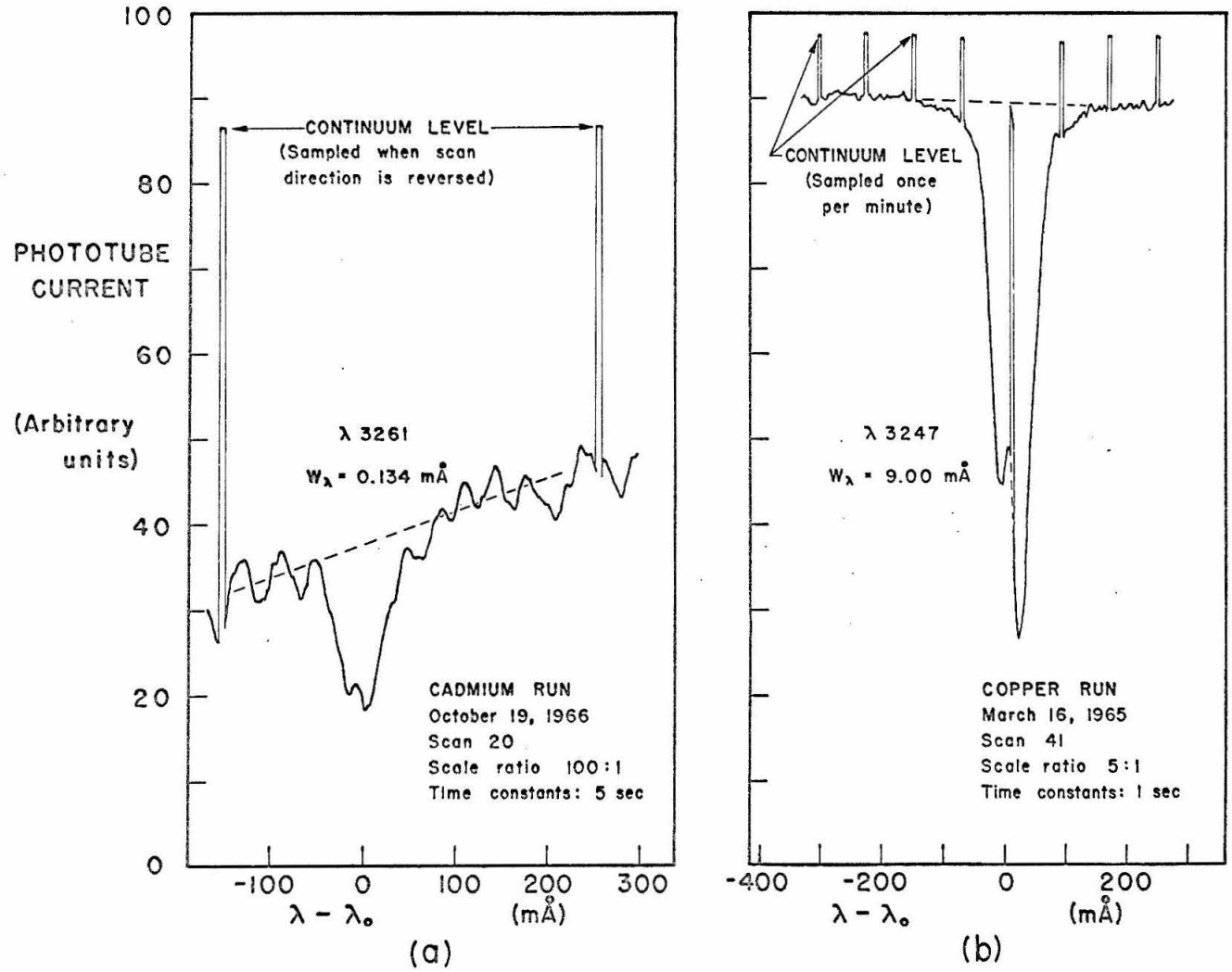

Figure 13. Equivalent width recordings.

IV DATA AND RESULTS

The procedure followed in obtaining the data is as follows:

Values of the various quantities relating to the geometry of the atomic beam are measured each time the furnace is assembled for a run. From these measurements Q is calculated using equation (51). After the vacuum system has been pumped down, the furnace is heated to produce an atomic beam and the phototubes are scanned back and forth over the line to record data on equivalent widths. Each scan takes about 5 minutes. During this time, the shutter under the microbalance pan is opened for a few minutes to record the deposit rate and recovery times, and the furnace temperature is measured. After the line has been scanned several times, the furnace temperature is changed and more scans are made. This is continued until data have been obtained for as wide a range of atomic beam densities as possible. Usually 20 to 30 scans are recorded for each line.

For each scan, values of W_λ, G, t_R, and T are obtained and a value of f is calculated as described in Section II-I. A weight is assigned to each measurement depending on the slope of the curve of growth in the region where the measurement was made and the apparent quality of the equivalent width and deposit rate data. The f-value is then calculated as the weighted mean of the individual measurements.

The experimental results are reported in the following Sections along with a discussion of methods and problems unique to each transition or element. For each line a curve of growth plot is

presented showing the theoretical curve and the experimental data. Each experimental point is a plot of the observed value of $W_\lambda/\Delta\lambda_D$ versus the corresponding observed value of $\bar{f} F_B F_G G/QT$ where $\bar{f}$ is the average f-value derived from all of the points.

A. Iron

Data are presented for the λ3720 transition $a^5D_4 - z^5F^o_5$. It was measured using the apparatus described by Lawrence[9] and Link[10] with which equivalent widths are measured by recording the difference between the light intensity at two wavelengths 6 Å apart. A single phototube alternately detects both signals which are chopped by a motor-driven shutter. One of the signals comes from the continuum and is used as a reference while the other scans the line.

Stabilized zirconia crucibles and tantalum furnace tubes were used because molten iron reacts with graphite. The diameter of the orifice was 2.0 mm. A radiation shield, made of 5 mil sheet tantalum, was placed around the furnace to reduce the power needed to reach the high temperatures at which iron vaporizes. Some trouble was experienced with iron droplets condensing at the orifice of the crucible and sometimes completely plugging it. This did not occur while the data reported here were obtained.

Since iron is magnetic, the pan damping magnet could not be used so damping was provided by sliding friction at the microbalance stirrup. Because of the extra noise introduced by motion at the stirrup, recovery time data were poor and were usually not taken.

The few recovery times that were measured show no significant difference from the theoretical values.

The pan heater consisted of a small tungsten lamp near the pan.

Iron has several low-lying energy levels which are appreciably populated at the furnace temperatures used. The states $a\ ^5D_{4,3,2,1,0}$ have energies of 0.00, 0.05, 0.09, 0.11, and 0.12 eV respectively. The Boltzmann factors range from 46% to 2.6% and are rather insensitive to the temperature. The next lowest states, $a\ ^5F_{5,4,3,2,1}$ have energies from 0.86 to 1.01 eV and are only very slightly populated.

At the temperatures at which data were obtained, the mean free path of the iron atoms inside the crucible varied from 0.18 to 3.3 times the orifice diameter. At these atomic beam densities the assumption of effusive flow is not wholly justified. Measurements of the effect this has on atomic beam f-values are discussed in Section IV-C for cadmium and a formula for correcting the data is given. The result is another factor F_L, which multiplies G in equation (50) along with F_B and F_G. These corrections increase the f-value of the Fe line λ3720 by 9%.

More than 91% of natural iron consists of the isotope ^{56}Fe, which has no nuclear spin and thus no hyperfine structure. In addition, the value of the damping ratio a' is negligibly small. Therefore, the single component curve of growth given by equation (32) was used.

Twenty-six scans were recorded for this line. Table I

Table I Fe λ3720 data

Quantity	Values(s)	Units
b	2.841	inch
z_o	1.170	inch
ρ	0.189	inch
$\sin \theta_o$	0.670	
Q	6.90×10^{-4}	$(\mu g/min)\ ^oK^{-1}$
T	2005 to 2230	^oK
$\Delta\lambda_D'$	6.42 to 6.77	mÅ
W_λ	1.55 to 11.72	mÅ
G	8.28 to 162.6	μg/min
F_B	0.460 to 0.447	
F_L	0.983 to 0.769	
f	0.0356 to 0.0534	

summarizes the data and Figure 15 shows the curve of growth. The weighted mean f-value is

$$f_{\lambda 3720} = 0.0430$$

with a standard deviation of the individual values of 6.8%.

This value is considerably larger than the value of 0.032 obtained by Bell, et al.[6] Part of the difference is accounted for

by the mean free path correction which has not been applied to previous atomic beam f-values. These may also have been some trouble in the earlier work with gas adsorption by the deposit on the micro-balance pan since a pan heater was not used. This is discussed for copper in the next section.

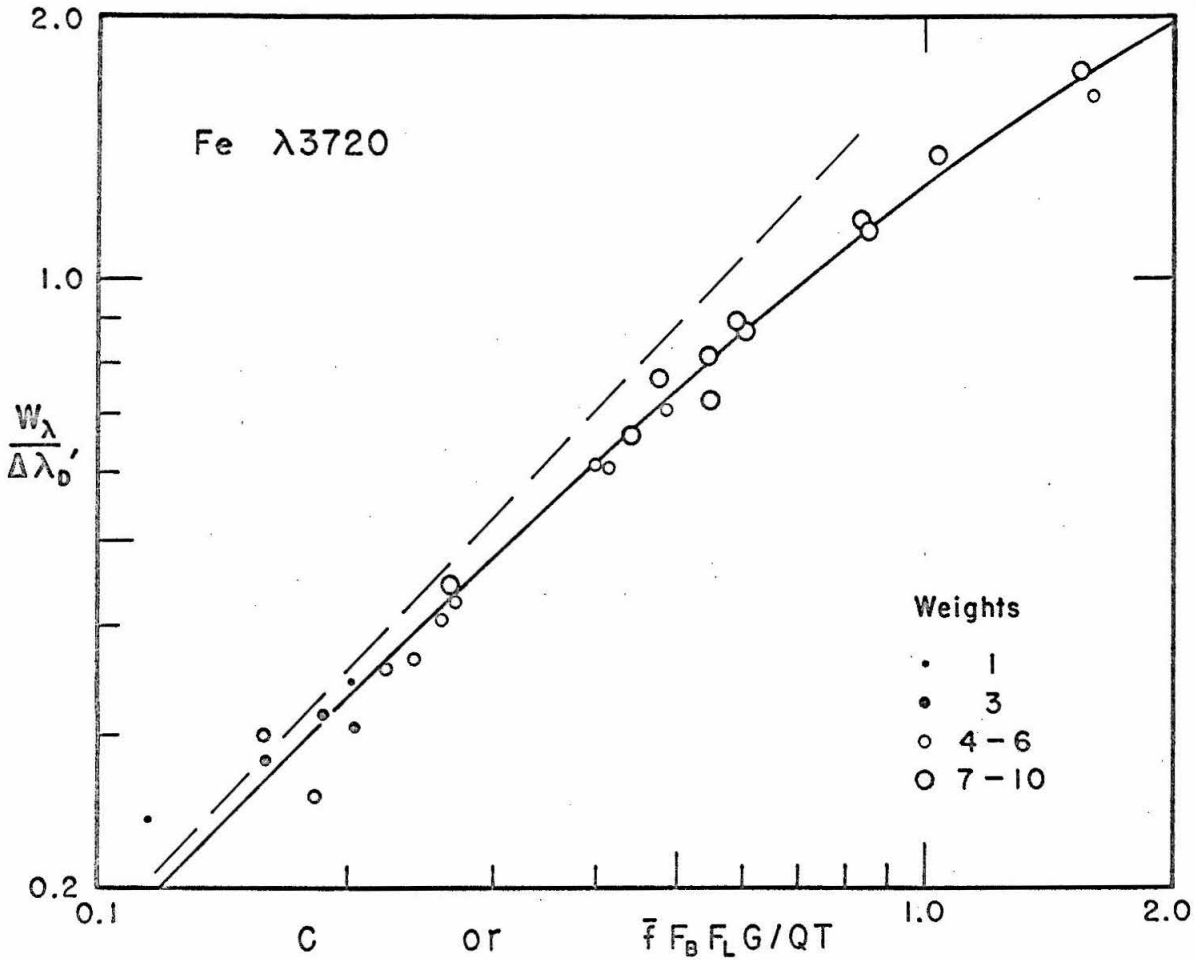

Figure 14. Theoretical curve of growth (solid line) for λ3720 of Fe. Dashed line is asymptotic to the linear part of the curve. Experimental data are plotted for $\bar{f}$ = 0.0430.

B. Copper

Copper behaves quite well in the atomic beam furnace, so it was used to test new apparatus as it was being developed. Molten copper does not react in any way with the graphite crucible, which may be reused indefinitely without any noticeable deterioration. Little trouble was experienced with droplets of metal condensing in the 1 mm diameter orifice except at very large atomic beam densities.

Although molecules have been observed in copper vapor, Nesmeyanov[19] states that their percentage is negligibly small. This is supported by the observed recovery times which show no systematic difference from the theoretical values.

Since the excitation potential of the first excited state of CuI is 1.38 eV, 99.9% or more of the atoms are in the ground state at the temperatures used and no Boltzmann factor is needed.

Oscillator strengths were measured for three lines of copper. In addition to the resonance doublet λλ3247, 3274 ($4s\ ^2S_{1/2} - 4p\ ^2P^o_{3/2,1/2}$), which was easily measured with the atomic beam apparatus, there are other doublets arising from the ground state at shorter wavelengths. All but one of these are too far in the ultraviolet to be measured with the present apparatus. Only the strongest line, λ2492 ($4s\ ^2S_{1/2} - 4p'\ ^4P^o_{3/2}$), of this doublet was measured.

Since λ2492 is an intercombination line with a small f-value, large atomic beam densities were needed to observe it.

Condensed droplets in the orifice were very troublesome. At these densities the mean free path of the atoms in the crucible is small so the correction factor F_L (see Section IV-C) must be applied. It has not been applied to the data for λ3247 or λ3274 since the densities were much smaller.

The intensity of the continuum at 2492 Å is about one tenth that at longer wavelengths which makes equivalent width measurements less accurate. The light output is also rather insensitive to the lamp voltage so difficulty was experienced with the power modulator circuit of the light regulator.

Copper has two stable isotopes: A = 63 (69% abundance) and A = 65 (31%). Both have nuclear spin 3/2. The hyperfine and isotopic splittings shown in Figure 15 were calculated from the tables of Landolt-Börnstein.[20] Each line is split into 8 or 12 components which are grouped so that the curve of growth given by equation (39) may be used. For λ2492 C is divided into 4 parts in the ratio 21 : 5 : 5 : 1 ; for λ3247 and λ3274 C is split 5 : 3. The approximate curves of growth obtained this way are sufficiently accurate for the data obtained but should be expected to diverge from the true curves for larger values of C.

Table II summarizes the copper data which is plotted in Figures 15, 16, and 17. The average f-values are

$$f_{\lambda 3247} = 0.427 \pm 6.1\% \quad \text{(std. dev. of individual values)}$$

$$f_{\lambda 3274} = 0.206 \pm 6.6\%$$

$$f_{\lambda 2492} = 0.0037 \pm 16\%$$

Bell, et al.[6] obtained 0.31 for the f-value of λ3247 compared to the value 0.427 obtained here. The difference appears to be due to the use of the pan heater. A series of f-value measurements, with and without the pan heater, was made to determine the magnitude of the effect. The result for λ3247 using the pan heater was 0.43, agreeing with the previous measurements, while 0.37 was obtained without the pan heater. Furthermore, the results without the pan heater showed a definite dependence on the atomic beam density, smaller observed f-values being obtained at smaller densities. This is consistent with the hypothesis that residual gases are adsorbed by the pan unless the pan heater is used to drive them off. The remaining difference is probably due to higher pressure in the vacuum chamber. The pressure during the measurements of Bell, et al. was 5×10^{-5} torr, which is ten times that attained here.

Much of the difference between the f-value measured here for iron and that measured by Bell, et al. is most likely due to the same effect. Similar differences exist in the f-values of chromium measured by Link[10] with a pan heater and by Bell[5] without a heater.

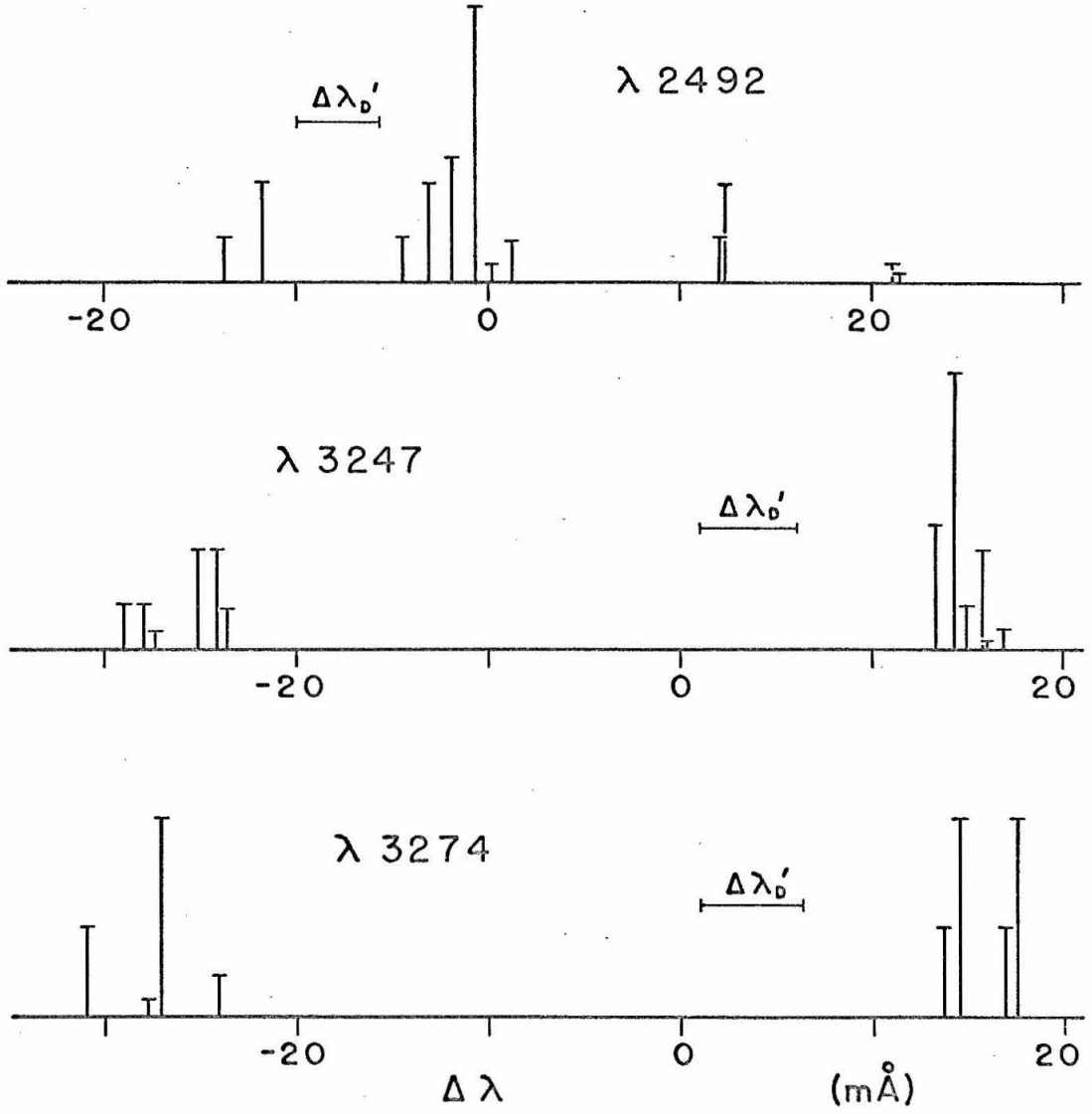

Figure 15. Hyperfine and isotopic splitting for copper.

Table II Copper data

Quantity	λ3247	λ3274	λ2492	Units
No. of scans	25	23	9	
b	2.773	2.773	2.773	inch
z_o	0.949	0.949	0.953	inch
ρ	0.288	0.288	0.288	inch
$\sin \theta_o$	0.733	0.733	0.733	
Q	1.548×10^{-3}	1.536×10^{-3}	2.026×10^{-3}	$(\mu g/min)\ {}^{o}K^{-1}$
T	1370 to 1770	1440 to 1806	1815 to 2023	${}^{o}K$
$\Delta\lambda_D'$	4.75 to 5.40	4.92 to 5.50	4.20 to 4.43	mÅ
W_λ	0.188 to 19.69	0.204 to 15.62	0.157 to 2.29	mÅ
G	0.124 to 22.46	0.286 to 35.4	25.2 to 578	μg/min
F_L	---	---	0.956 to 0.644	
f	0.328 to 0.502	0.182 to 0.273	0.00297 to 0.00535	

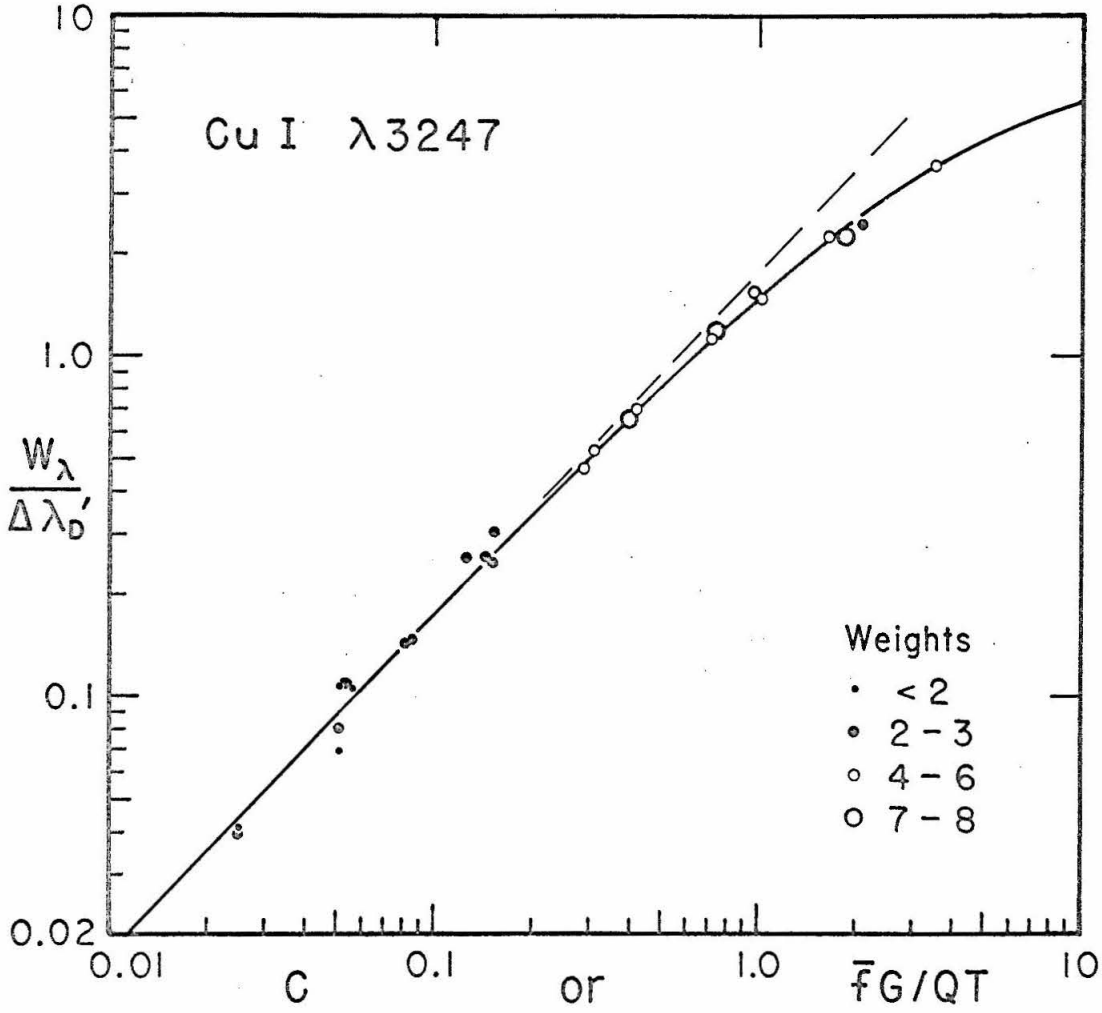

Figure 16. Theoretical curve of growth and experimental data for λ3247 of Cu with $\bar{f}$ = 0.427.

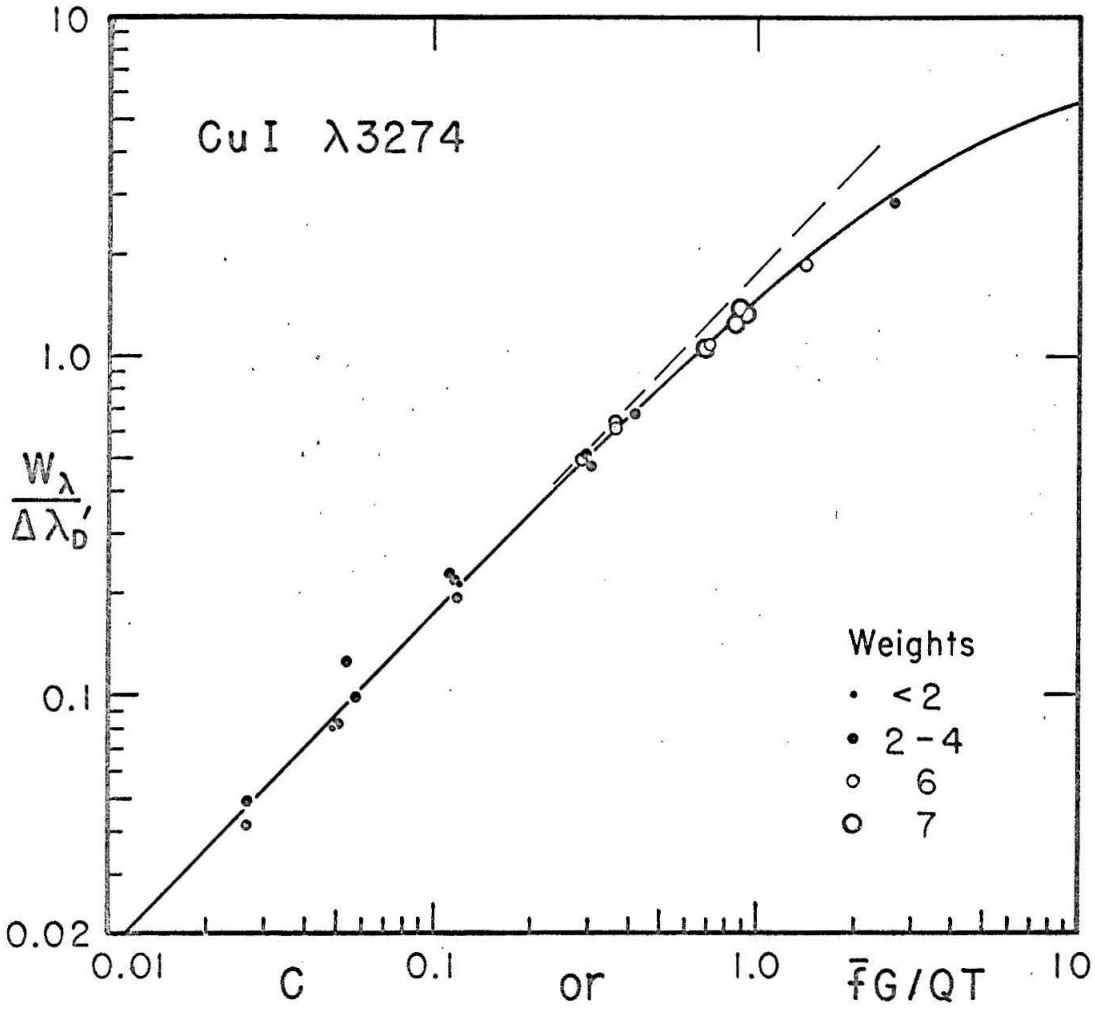

Figure 17. Theoretical curve of growth and experimental data for λ3274 of Cu with $\bar{f}$ = 0.206.

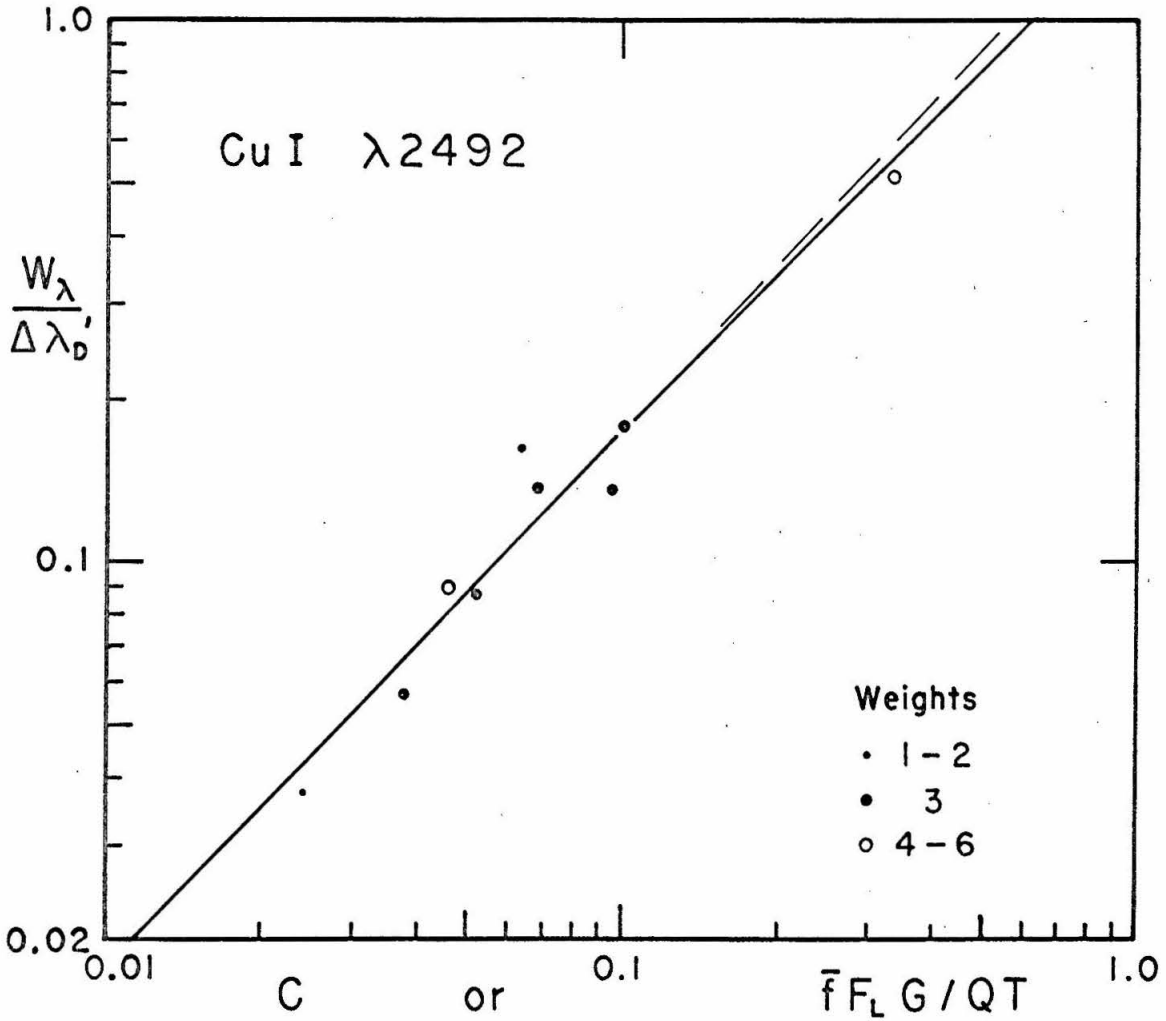

Figure 18. Theoretical curve of growth and experimental data for λ2492 of Cu with $\bar{f}$ = 0.0037.

C. Cadmium

Cadmium forms a useable atomic beam at temperatures as low as 200°C. The special crucible and thermocouple used to measure the temperature have been described in Section III-B. Because of the low furnace temperatures, outgassing was greatly reduced and the pressure in the vacuum chamber was always less than 10^{-6} torr and usually between 1 and 3 x 10^{-7} torr. This is a factor of 10 lower than for other elements.

In accordance with its high vapor pressure, atoms of cadmium do not always stick when they impinge on a surface at room temperature. For example, Nesmeyanov[19] states that temperatures of -185 to -78 °C are suitable for condensing cadmium vapor compared with +350 to +575 °C for copper vapor.

This has two effects in the atomic beam apparatus. First, part of the atomic beam bounces back through the light beam from nearby surfaces, increasing the absorption over that due to the atomic beam alone; and second, the deposit rate measured by the microbalance is too low. The latter effect can be corrected for if recovery times are measured, but it is desirable to minimize this correction. The first effect must be eliminated as there is no way to calculate it. This was done by extending an auxiliary liquid nitrogen cold trap under the plate containing the aperture beneath the balance pan. All of the atomic beam is condensed on this cold trap except for a small portion which goes through a hole in the

trap to the aperture and balance pan. The effectiveness of the cold trap was demonstrated by the fact that cadmium no longer condensed on everything else in the vacuum chamber after the trap was installed.

The problem of atoms bouncing off the pan was largely solved using the pan heater. The heater could not be used in the usual manner while the deposit rate was being measured as it would have evaporated the deposit. However, if the pan was heated for a few minutes and then immediately exposed to a rather intense atomic beam, subsequently measured recovery times indicated that 98 to 99 % of the atoms were sticking. Apparently the pan becomes covered with a contaminant on which cadmium atoms do not readily stick. For example, as much as 80% of the incident atomic beam has been observed to reflect off a new, unheated pan. The heater drives off this contaminant leaving a clean metal surface on which the atoms do stick.

Cadmium has an isolated ground state so no Boltzmann factor is needed. Only two lines from this state are accessible to the atomic beam apparatus: the resonance line $\lambda 2288$ ($5s^2\ {}^1S_0 - 5p\ {}^1P^o_1$), and the intercombination line $\lambda 3261$ ($5s^2\ {}^1S_0 - 5p\ {}^3P^o_1$).

Because the light level at 2288 Å was quite low, the amount of noise in the photocurrent was about 5 times greater than normal and the smallest equivalent widths that could be measured were about 0.5 mÅ. Coupled with the small Doppler width, this meant that data could be obtained only above the linear part of the curve of growth. Even if weaker lines could have been measured, the deposit rates would have been too small to measure because of the large f-value.

Tests with filters which cut out the far ultraviolet and pass longer wavelengths indicated the presence of a significant amount of scattered light at 2288 Å. To obtain a quantitative measurement of the scattered light a more selective filter, which absorbed light only in the immediate region of 2288 Å and passed everything else, was made by sealing a small quantity of cadmium in a quartz cell. This was wrapped with asbestos and nichrome heater wire, placed in the light path, and heated until the cadmium vapor in the cell produced an absorption line so strong that a region of approximately 2 1/2 Å was completely absorbed. Measurements of the residual intensity at the center of this line, which could only come from scattered light, showed that 12.6% of the total photocurrent without the cell was due to scattered light. To take this into account, the measured continuum level was decreased by this amount in the process of reducing the equivalent width data.

Cadmium has eight stable isotopes of which two have nonzero nuclear spin and thus exhibit hyperfine structure. The structure of λ3261 was measured by Kelly and Tomchuk.[21] That of λ2288 has been deduced from the isotope shifts of ^{110}Cd, ^{112}Cd, and ^{114}Cd, also measured by Kelly and Tomchuk.[22] The shifts for the other isotopes were determined by a fit with the shifts measured by Kuhn and Ramsden[23] for λ4416 of Cd II. Finally, the hyperfine splitting of ^{111}Cd was taken from the work of Lurio and Novick[24] and the splitting of ^{113}Cd was obtained from this using the nuclear magnetic moment ratio measured by Procter.[25]

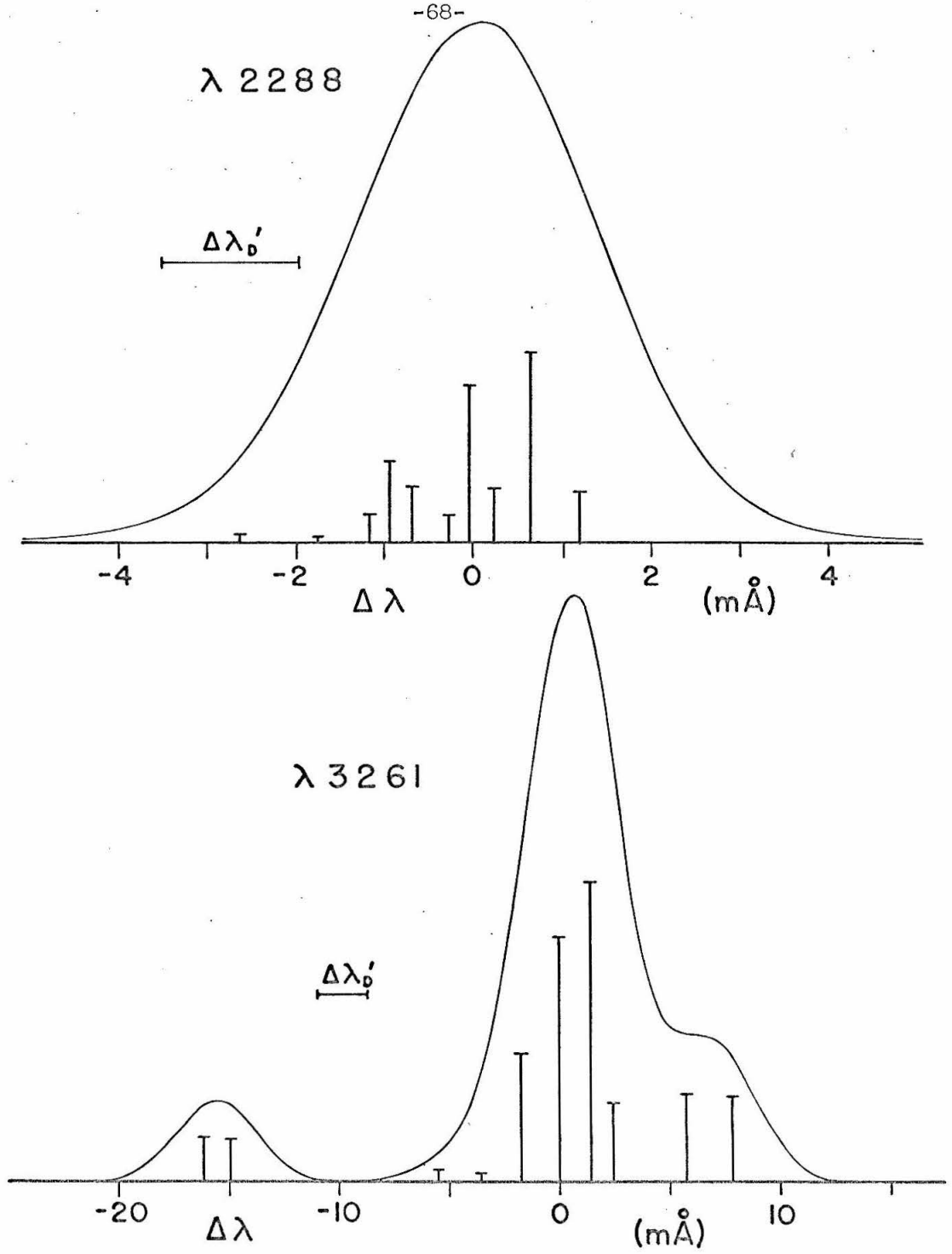

Figure 19. Hyperfine and isotopic splitting for cadmium.

The resulting splittings are shown in Figure 19 along with the line profiles with appropriate Doppler widths. It can immediately be seen that there is no valid way to group the components of either line so that the approximation of equation (39) can be used. For both lines, accurate curves were calculated by evaluating equation (38) numerically. This was not necessary for λ3261 since all the data were obtained on the linear part of the curve and even a very poor approximation to the true splittings produces accurate results here. However, for λ2288 the accurate curve is a necessity as all the data falls above the linear part.

The value of a' for λ3261 is 0.00005, which can certainly be set equal to zero. For λ2288, using $f = 1.38$ and $\Delta\lambda_D' = 1.6$ mÅ, equation (49) yields $a' = 0.0510$. The value assumed to compute the curve of growth was 0.0536. Since the value of a' affects only the upper part of the curve, where there are only a few data points, this difference is not serious. It is estimated that it changes the f-value derived from the data by less than 0.5%.

The λ3261 it was necessary to use large deposit rates because the f-value is so small. At these high densities the mean free path of the atoms inside the crucible is not large compared to the orifice diameter. When the individual f-value measurements were calculated by the relation

$$f' = QTC/F_G G \quad , \tag{52}$$

there was a definite tendency for lower values of f' to be obtained at

larger deposit rates. This is probably due to a breakdown, at high vapor densities, of the assumption that the atomic beam is formed by effusive flow.

No theoretical expression is available for the atomic beam density in this case, but it is reasonable to assume that f' is a function only of the mean free path and approaches the true f-value as the mean free path becomes large. The f-value can, therefore, be obtained by extrapolation.

The mean free path in a gas of n_o atoms/cm^3 is given by Kennard[12] as

$$L = \frac{1}{\sqrt{2}\,\pi\,\delta^2\,n_o} \tag{53}$$

where δ is the atomic diameter. There is a question as to the choice of δ. Probably, values of δ based on transport phenomena (viscosity or heat conductivity) would be best if they were available. However, in order to get comparable values for different elements, values slightly larger than the nearest neighbor distance in the solid state have been used here. For cadmium, the value $\delta = 3.2$ Å was chosen.

Equation (53) can be combined with equations (2), (3), and (34) to give

$$L = \frac{d^2}{8\,N_o\,\delta^2}\,\sqrt{MR/\pi}\,\left(\frac{\rho^2}{b^2+\rho^2}\right)\frac{\sqrt{T}}{G} \tag{54}$$

where d is the diameter of the crucible orifice. For cadmium d was 0.19 cm.

It is most convenient to plot the data versus the dimensionless quantity d/L given by

$$d/L = \frac{8 N_o \delta^2}{d} \sqrt{\pi/MR} \left(\frac{b^2 + \rho^2}{\rho^2} \right) G/\sqrt{T} \qquad (55)$$

and extrapolate to zero d/L to get the value of f. This is done in Figure 20. Instead of f', log f' has been plotted as the ordinate because it was thought that this would enable a straight line extrapolation to be made.

The plot shows considerable scatter so the data were averaged in six groups having d/L ranging from 0-1, 1-2, 2-4, 4-6, 6-10, and 10-20. These averages are plotted as the square symbols with error bars. A straight line (the dashed line in Figure 20) was fitted to these points by the method of least squares. The result is

$$\log f' = -2.749 - 0.0151 (d/L) \quad .$$

The value of χ^2 is 10.5, which for 4 degrees of freedom has only a 3% probability of occurance. The reason for the bad fit is obvious; the curve should be concave upward. Therefore, the points were fitted with a quadratic with the result:

$$\log f' = -2.730 - 0.0249 (d/L) + 0.00080 (d/L)^2 \quad .$$

This is the solid line in Figure 20. The value of χ^2 is 7.4 with a probability of getting this or larger of 6% (3 degrees of freedom). This is somewhat better.

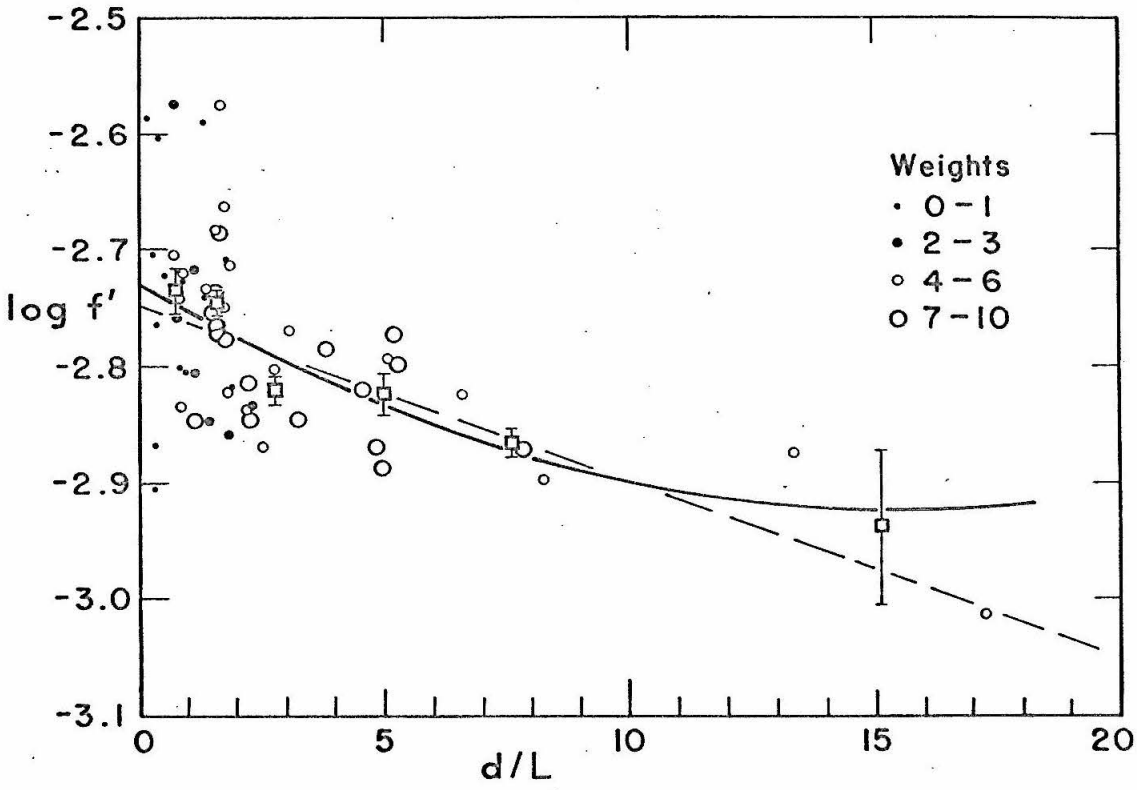

Figure 20. Mean free path correction. The apparent f-value, calculated from $f' = QTC/F_G G$, is plotted versus the ratio d/L of the orifice diameter to the mean free path of the atoms inside the crucible. Square symbols are averages for points having d/L in the ranges 0-1, 1-2, 2-4, 4-6, 6-10, 10-20. Dashed line is a linear fit to these points; solid line is a quadratic fit.

Because data for other elements are sometimes also obtained at large deposit rates, a correction has also been applied to them. It is assumed that f' has the same dependence on d/L as observed for cadmium so that the correction can be made by multiplying each value of G by

$$F_L = \text{antilog}\,[-\,0.0249\,(d/L) + 0.00080\,(d/L)^2\,] \quad . \qquad (56)$$

Individual measurements of f-values are thus obtained from

$$f = \frac{QTC}{F_B F_G F_L G} \quad . \qquad (57)$$

Since the data on which this correction is based show considerable scatter, and since the actual form of the correction has not been confirmed for other elements, it can not be regarded as being very accurate. Certainly it is not valid for $d/L > 20$. Nevertheless, to neglect it would result in systematic errors. The validity of the correction is corroborated by the fact that in every case where it has been applied the scatter of the data has been reduced.

The data for the cadmium lines are summarized in Table III and plotted in Figures 21 and 22. The average f-values and the standard deviation of the individual measurements are:

$$f_{\lambda 3261} = 0.00190 \pm 14.6\%$$

$$f_{\lambda 2288} = 1.38 \pm 25.6\%$$

These values are larger than the values which would have been obtained without the mean free path correction by 15.7% for λ3261 and 1.7% for λ2288. The large deviations are due to the reasons discussed above, i.e. small equivalent widths for λ3261, and low light level and small curve of growth slope are λ2288.

Table III Cadmium data

Quantity	λ3261	λ2288	Units
No. of Scans	58	29	
b	2.786, 2.790	2.785	inch
z_o	1.029, 1.032	0.985	inch
ρ	0.3024	0.3024	inch
$\sin \theta_o$	0.716, 0.709	0.717	
Q	1.830×10^{-3}, 1.829×10^{-3}	2.499×10^{-3}	$(\mu g/min)\ ^oK^{-1}$
T	545 to 693	475 to 620	^oK
$\Delta\lambda_D'$	2.21 to 2.47	1.45 to 1.66	mÅ
W_λ	0.059 to 2.21	0.496 to 13.94	mÅ
G	0.950 to 580	0.191 to 142.9	μg/min
F_G	0.972 to 5.11*	0.906 to 1.077	
F_L	0.988 to 0.644	1.000 to 0.826**	
f	0.00127 to 0.00277	0.87 to 2.02	

* Five measurements before the pan was cleaned with the pan heater had F_G ranging from 5.11 to 1.438. All others had $F_G \leq 1.30$.

** Most values are nearly unity, only 3 are less than 0.95.

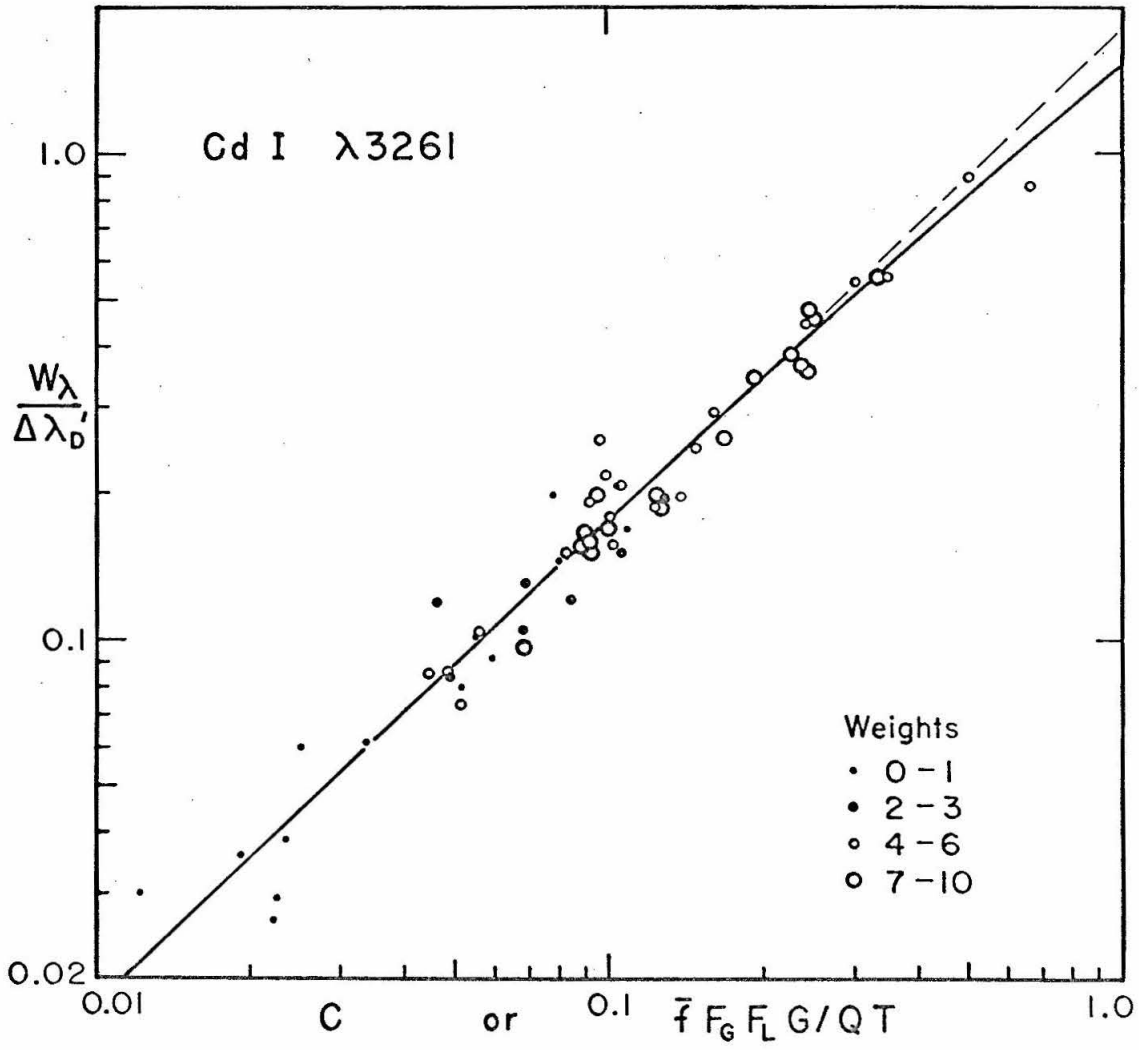

Figure 21. Theoretical curve of growth and experimental data for λ3261 of Cd.

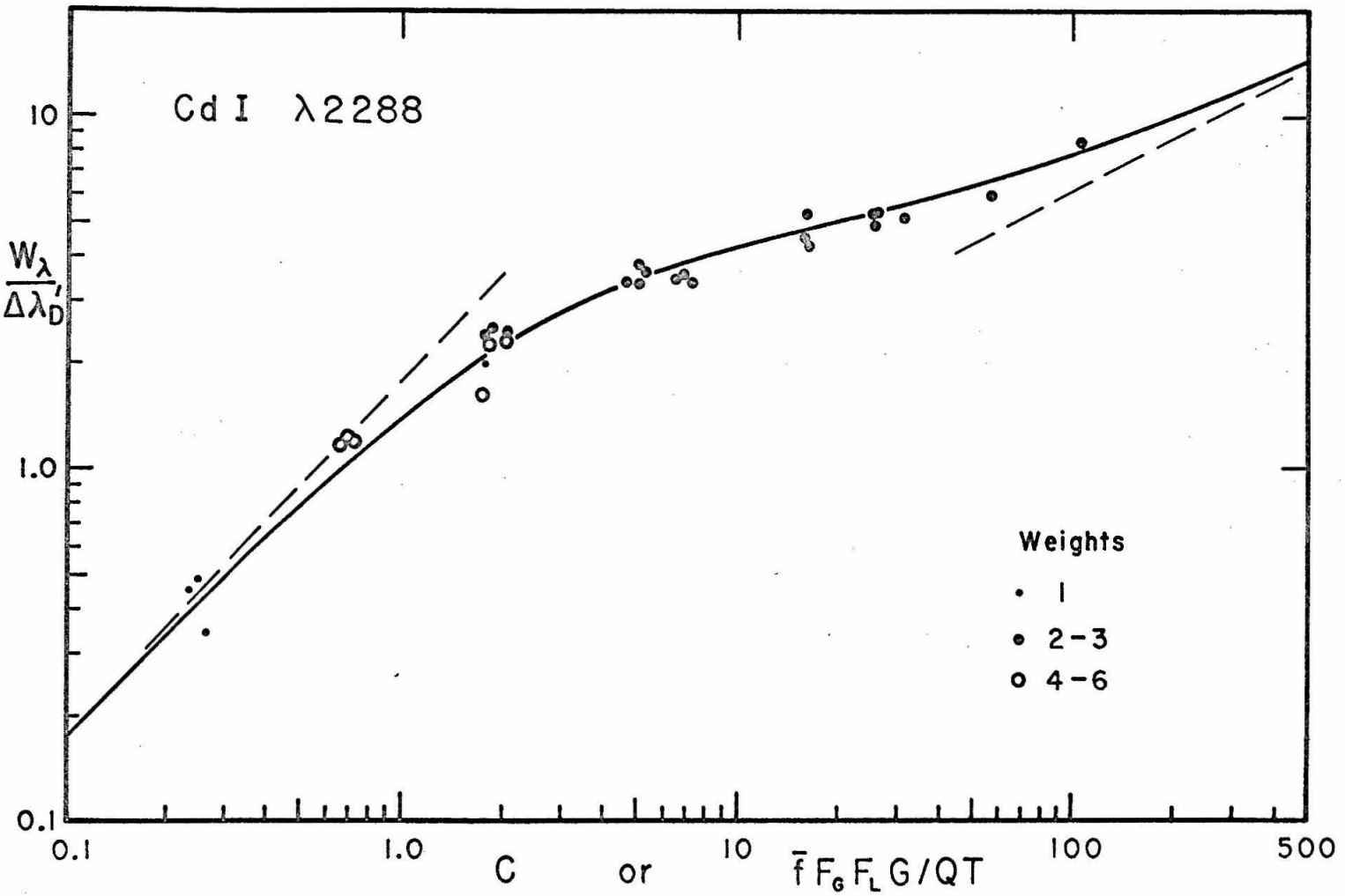

Figure 22. Theoretical curve of growth and experimental data for λ2288 of Cd.

D. Gold

The two gold resonance lines λλ2428, 2676 ($6s\ ^2S_{1/2}$ - $6p\ ^2P^o_{3/2,1/2}$) are analogous to the copper resonance lines. G. M. Lawrence[9] measured λ2676 with the atomic beam and obtained an f-value of 0.125, but, apparently because the optical system was not properly focused, the light level was much too low to measure the f-value of λ2428. The present measurements have been largely limited to this line.

Gold was evaporated from a graphite crucible with a 1.0 mm orifice. No trouble was experienced with droplets condensing in the orifice. However, the recovery times ranged from nearly 40% too long at low deposit rates to 20% too short at the largest deposit rate. This indicated trouble with both the sticking coefficient and gas adsorption. Because the furnace had been outgassed for 36 hours at temperatures slightly below that which produces an appreciable atomic beam, the pressure was as low as 6×10^{-7} torr for small deposit rates. However, it rose to 5×10^{-5} torr at the highest furnace temperature. This explains why adsorbed gas caused more trouble at larger atomic beam densitites. The sticking coefficient seemed to slowly improve with time.

In correcting for the abnormal recovery times, values of $1/(1 + \Lambda)$ ranging from 0.69 (corresponding to non-unity sticking coefficient) down to 0.54 (gas adsorption) were used depending on which effect predominated. Despite the fact that the corrections were

as large as 27%, the individual f-value measurements show little scatter and no variation with atomic beam density.

Gold consists entirely of one isotope, ^{197}Au, which has a nuclear spin of 3/2. Elliott and Wulff[26] found that λ2428 has two hyperfine components with intensities in the ratio of 5:3 and separated by 12.6 mÅ. Since this separation is more than 5 times the Doppler width, the curve of growth is accurately given by equation (39).

The intensity of the mercury lamp, while somewhat low at 2428 Å, is sufficient to allow accurate measurements of equivalent widths. Measurements with filters indicated the presence of a small amount of scattered light. This was corrected for by reducing the observed continuum intensity by 2 1/2%.

The first excited state of gold is 1.13 eV above the ground state and is populated by from 0.2 to 0.5% of the atoms at furnace temperatures of 1750 to 2050 °K. The corresponding Boltzmann factors for the ground state are nearly unity.

Mean free path corrections have been applied to the data although the deposit rates were usually small enough so that this had little effect. At the largest atomic beam density the correction was nearly 8%, but for most of the measurements it was less than 1%.

The data for λ2428 are summarized in Table IV and plotted in Figure 23. The weighted mean f-value and standard deviation of 20 measurements are

$$f_{\lambda 2428} = 0.283 \pm 6.2\% \quad .$$

Three scans were made of λ2676 with results that were consistent with the f-value of 0.125 previously obtained by Lawrence.

Table IV Au λ2428 data

Quantity	Value(s)	Units
b	2.777	inch
z_o	0.998	inch
ρ	0.3024	inch
$\sin \theta_o$	0.725	
Q	2.400×10^{-3}	$(\mu g/min)\ {}^{o}K^{-1}$
T	1759 to 2042	^{o}K
$\Delta\lambda_D'$	2.26 to 2.44	mÅ
W_λ	0.758 to 8.90	mÅ
G	2.35 to 70.9	μg/min
F_B	0.998 to 0.995	
F_G	1.272 to 0.893	
F_L	0.997 to 0.927	
f	0.246 to 0.326	

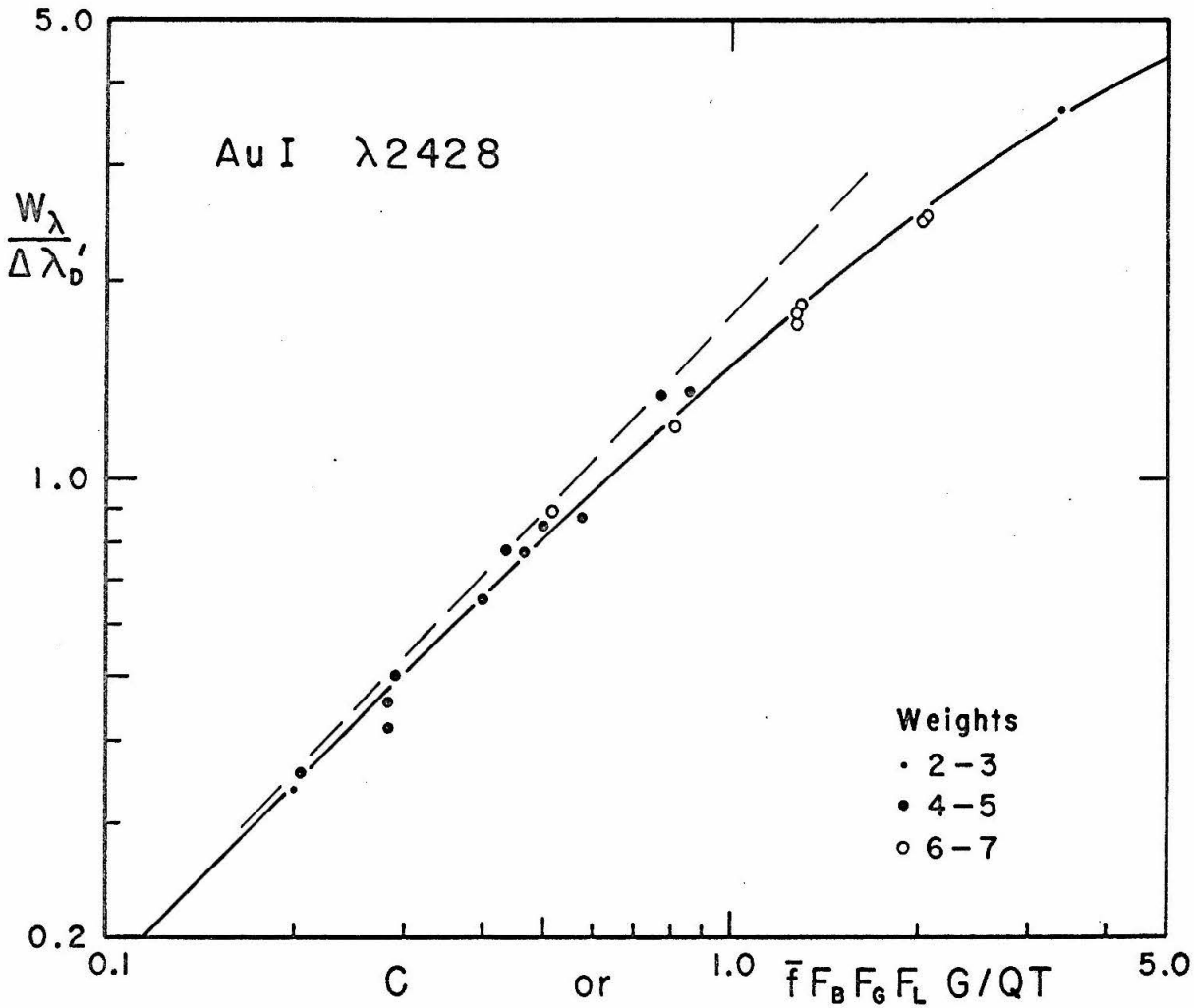

Figure 23. Theoretical curve of growth and experimental data for λ2428 of Au.

V ACCURACY OF RESULTS

It has always been difficult to assign error limits to absolute f-value measurements because of the possibility of unsuspected systematic errors. For earlier atomic beam measurements, such errors have been present because of scattered light in the spectrograph, gas adsorbed by the deposit on the balance pan, and deviations from effusive flow. Where applicable, appropriate corrections have been made for these effects in this work. The possibility remains, however, that these corrections may be of the wrong magnitude or that other effects may be present.

Most of the random errors arise in the measurement of equivalent widths and are caused by statistical noise in the phototube signal. For easily measured f-values, the random error of a single measurement has a standard deviation of 6 to 7%. Since 20 to 30 measurements are usually averaged together for each f-value determination, the standard deviation of the mean is about 1.4% or less.

Oscillator strengths are calculated from equation (57):

$$f = \frac{QTC}{F_B F_G F_L G} \quad .$$

Estimates of the systematic errors in the quantities in this formula are given below.

Q: This factor contains most of the measurements of the geometry of the atomic beam and is given by equation (51):

$$Q = \left(\frac{2 R m c}{N_o e^2 \lambda_o} \right) z_o \left(\frac{\rho^o}{b^2 + \rho^2} \right) .$$

The values of b and z_o were about 2.8 and 1.0 inch respectively and could be measured with an accuracy of at least 0.005 inch. Various values of ρ between 0.19 and 0.30 inch were used, each measured with an accuracy of 0.001 inch. The estimated uncertainly in Q is 0.7 to 0.8%, which is the square root of the sum of the squares of the errors due to b, z_o, and ρ.

T: The temperature is involved in a more complicated manner than is indicated by equation (57) since C depends on $W_\lambda / \Delta\lambda_D'$ and the Doppler width $\Delta\lambda_D'$, in turn, is dependent on T. On the linear part, the curve of growth is given by equation (32) using only the first term of the series. If this is combined with equation (48) for the Doppler width and the resulting expression for C is put into equation (57), it is seen that the f-value is proportional to the square root of the temperature. As the curve of growth flattens out, T has even less effect on f.

Temperatures measured with the optical pyrometer should have systematic errors of no more than 20^o. At 1400 ^oK the error in f is 0.7%. The thermocouple used to measure the furnace temperature for cadmium has an estimated error of 10^o or less, which produces an error of 0.8% in f at 600 ^oK.

C: On the linear part of the curve of growth, C is proportional to $W_\lambda / \Delta\lambda_D'$. The following are sources and estimated

maximum values of errors in equivalent width measurements: 2.0% from amplifiers, range switches, and chart recorder; 2.5% from scanning speed; 0.4% from planimeter calibration; and 1.0% from scattered light. These combine to give 3.4% as the error in W_λ.

The Doppler width is proportional to $\sqrt{T}$ and sin θ_o. The effects of errors in T have already been accounted for. The angle θ_o is determined by the width and height of the slot in the water jacket surrounding the furnace. Uncertainties in the position of the orifice and in the actual width of the slot, which is narrowed by deposits from the atomic beam, limit the accuracy of sin θ_o to 1.0%.

Combining the above figures, the error in $W_\lambda/\Delta\lambda_D'$ is 3.5%. On the linear part of the curve of growth, the error in C is the same, but on the knee or above, this value should be increased by dividing it by the slope of the curve. For most lines this slope is between 1.0 and 0.8, but for Cd λ2288 the average slope is about 0.33, and the error in C due to errors in $W_\lambda/\Delta\lambda_D'$ is 11%.

In all cases where the approximate treatment of hyperfine and isotopic splittings was not sufficient, an accurate curve of growth was calculated from equation (38). Therefore, errors in C due to this cause should be negligible. The assumption that the light beam has no height and width as it traverses the atomic beam leads to a maximum error of 0.8%.

G: The microbalance was calibrated with a 1.0 mg, class M weight, which has a specified error of less than 0.54%. Five such weights were compared on the microbalance and the difference between

the heaviest and lightest was only 0.25%. The microbalance electronics, range switch, and chart recorder should be accurate to within 1.0%. Other errors in determining the deposit rate from the chart recording should be random in nature, so the systematic error in G is less than 1.1%.

F_B: Cu, Cd, and Au, which have Boltzmann factors near unity, have no errors due to this source. For Fe, a 20° error in temperature leads to a 0.3% error in F_B. However, G. M. Lawrence[9] finds evidence that the actual populations of the states may correspond to a temperature 300° or 400° lower than the furnace temperature. If true, this would lead to nearly a 5% error in F_B for iron.

F_G: The accuracy of this factor depends on the accuracy with which recovery times can be measured (1.0%) and the accuracy of $1/(1 + \Lambda)$. Because of uncertainties about the value of $1/(1 + \Lambda)$, errors in f from this source will be assumed to be 1/4 of the amount that F_G changes the f-value.

F_L: The mean free path correction has not been accurately established. Therefore, errors in f will be assumed to be 1/3 of the amount F_L changes f for cadmium, and 1/2 of the change for all other elements. For the two strong copper lines, this correction was small and was not used. In this case, the error is assumed to be equal to the change the correction would have made in the f-value.

The estimated errors in each of the relevant quantities are given in Table V for each line measured. The last column gives the square root of the sum of the squares of these errors for each line.

These values are thought to be good estimates of the standard errors of the measured f-values. However, it cannot be definitely said that there are no other, undetected, systematic errors.

Table V Errors in f

Element and Wavelength	f-value	Random Errors (%)	Systematic Errors (%)							Standard Error of f (%)
			Q	T	C	G	F_B	F_G	F_L	
Fe 3720	0.0430	1.4	0.8	0.7	4.3	1.1	4.7	1.0	4.4	8
Cu 3247	0.427	1.2	0.7	0.7	3.9	1.1	0	1.0	0.9	4.5
3274	0.206	1.4	0.7	0.7	3.9	1.1	0	1.0	1.3	4.7
2492	0.0037	5.7	0.7	0.7	3.6	1.1	0	1.0	5.6	9
Cd 3261	0.00190	1.9	0.7	0.8	3.6	1.1	0	2.8	5.2	7
2288	1.38	4.8	0.7	0.8	11.0	1.1	0	1.1	0.6	12
Au 2428	0.283	1.4	0.7	0.7	4.1	1.1	0	2.5	0.9	5.3

VI COMPARISON WITH OTHER MEASUREMENTS

Oscillator strengths may be measured by a wide variety of different methods. Some of the more important ones are indicated below. Most of them are described in greater detail by Foster.[1]

Absorption cell: The light absorbed is compared with the number of absorbing atoms. Accurate vapor pressures are needed if absolute f-values are to be obtained; otherwise relative values may be measured.

Atomic beam absorption: Absorption is measured as above, but the number of absorbing atoms is measured directly.

Hook method: Similar to absorption cell except the anomalous dispersion of the refractive index in the region of the line is measured instead of the absorption. The name refers to the characteristic shape of the interferometer fringes. Vapor pressure data are needed to get absolute values.

Arc emission: Relative f-values are derived from the intensities of emission lines. Absolute values may be obtained by fitting the relative scale to known absolute values. Although this method is not very accurate, it is important because of the large number of lines for which it is the only method that has been used.

Corliss and Bozman[27] have measured the f-values of 25,000 lines of 70 elements using a copper arc containing a small percentage of the element being investigated. The f-values measured with the atomic beam by Bell et al.[6] for λ3720 of Fe and λ3247 of Cu were

among those used by Corliss and Bozman to normalize their relative scale. Since the values obtained in this investigation are larger than the values obtained by Bell et al., the f-values of Corliss and Bozman should perhaps be increased slightly. However, Allen and Corliss[28] suggest that they be decreased by 11%. This correction has not been applied to the values quoted here.

Lifetime: The mean lifetime of the excited state is measured by observing the decay of the emitted radiation or by modulating the exciting signal and observing the phase shift of the modulation of the emitted light.

Level crossing: Also called Hanle effect or magnetic depolarization. This method also measures the lifetime of the excited state.

Lifetime measurements have the advantage that it is not necessary to know the number of excited atoms. This is a major source or error in most other methods.

Absolute f-values can be derived from lifetime measurements using equations (27) and (28). If there is more than one downward transition from the excited state, relative f-values for all the transitions are needed.

Comparisons of f-values measured by different techniques, and, to a lesser extent, values measured by the same method, often show large discrepancies, sometimes by as much as a factor of 100 or more. For this reason, agreement between values measured by several methods must be obtained before they can be trusted.

Iron: Absolute f-values of the iron resonance line, as measured by various investigators, are collected in Table VI. There is general agreement that the f-value is between 0.03 and 0.06, but the scatter within this range is fairly large. In view of the astrophysical importance of this line, which is used to calibrate relative f-value scales to obtain absolute values for other lines, further measurements are needed.

Copper: The results are compared with other measurements in Table VII. For the resonance line λ3247, there is very good agreement between the present atomic beam measurement and recent lifetime measurements by both the level crossing and phase shift methods. It is perhaps significant that these are precisely the experiments that do not require accurate knowledge of vapor pressures.

Very few measurements of the line λ2492 have been made and the agreement between them is poor. The present determination is the first absolute measurement; all previous measurements give relative values which have been adjusted to an absolute scale by comparison with other f-values.

Cadmium: Other measurements and the present results are collected in Table VIII. The intercombination line λ3261 has been measured by many different methods with excellent agreement between most of them. This line is particularly suitable for lifetime measurements because of the relatively long-lived ($\tau = 2.4 \times 10^{-6}$ sec) upper state. Since it vaporizes at low temperatures, the vapor

Table VI

Oscillator Strengths for Fe λ3720

Observer	Method	f-value
King (1942)[29]	Absorption cell	0.013
King (1942, revised (1958)[6]	As above, new vapor pressure data	0.030
Kopfermann and Wessel (1951)[3]	Atomic beam absorption	0.043 ± 20%
Allen and Asaad (1957)[30]	Cu arc emission	0.034
Hinnov and Kohn (1957)[31]	Flame emission	≥ 0.046
Ziock (1957)[32]	Lifetime, phase shift	0.046 ± 30%
Bell et al. (1958)[6]	Atomic beam absorption	0.032 ± 12%
Addink (1959)[33]	Arc emission	0.0018
Ottinger and Ziock (1961)[34]	Lifetime, phase shift	0.035 ± 10%
Corliss and Bozman (1962)[27]	Cu arc emission	0.058
Morozova and Startsev (1964)[35]	Cu arc emission	0.045
Corliss and Warner (1964,66)[36,37]	Average of previous results	0.053
This investigation (1967)	Atomic beam absorption	0.0430 ± 8%

Table VII Oscillator strengths for copper

Observer	Method	f-values		
		λ3247	λ3274	λ2492
King & Stockbarger(1940)[38]	Absorption cell	0.62	0.32	
King & Stockbarger(1940), revised(1958)[6]	Same, but with new vapor pressures.	0.42	0.22	
Ostrovskii & Penkin(1957)[39]	Hooks	0.74	0.38	
Ostrovskii & Penkin(1957), revised(1963)[40]	Same, but with new vapor pressures	0.66	0.34	
Bell et al.(1958)[6]	Atomic beam absorption	0.31 ± 10%	0.16 ± 25%	
Addink(1959)[33]	Arc emission	0.13		
Vidale(1960)[41]	Absorption tube	0.32		
Corliss & Bozman(1962)[27]	Cu arc emission	0.32	0.155	0.0145
Riemann(1964)[42]	Arc emission	0.287 ± 14%	0.14 ± 14%	
Stewart & Rotenberg(1965)[43]	Theoretical: Scaled Thomas-Fermi	0.62		
Ostroumenko & Rossikhin(1965)[44]	Flame absorption			0.0057*
Moise(1966)[45]	Absorption cell	0.322	0.153	
Slavenas(1966)[46]	Hooks	0.66✓	0.323 ± 1.3%✓	0.0091 ± 3%✓
Ney(1966)[47]	Level Crossing	0.445 ± 3%‡		
Levin & Budick(1966)[48]	Level Crossing	0.43 ± 10%‡		
Cunningham & Link(1967)[49]	Lifetime - Phase shift	0.432 ± 4%‡		
This investigation (1967)	Atomic beam absorption	0.427 ± 4.5%	0.206 ± 4.7%	0.0037 ± 9%

* Ostroumenko and Rossikhin give relative values. The value quoted results from fitting their relative values to the absolute values for λλ3247,3274 given by this investigation.

✓ Slavenas measured relative values and normalized them so that $f_{\lambda 3247}$ was the same as that given by Ostrovskii and Penkin, revised.

‡ These investigators measured lifetimes. A branching ratio of 0.984 ± 0.007 was derived from the relative f-values of Corliss and Bozman to convert lifetimes to oscillator strengths for λ3247.

Table VIII Oscillator strengths for cadmium

Observer	Method	f-values	
		λ3261	λ2288
Kuhn(1926)[50]	Magneto-rotation	0.0019 ± 10%	1.20 ± 4%
Soleillet(1928)[51]	Magnetic depolarization	0.0024	
Ellett(1929)[52]	Magnetic depolarization	0.0021	
Zemansky(1931)[53]	Absorption cell		1.19
Koenig & Ellett(1932)[54]	Lifetime	0.0019 ± 10%	
Soleillet(1933)[55]	Lifetime	0.00195	
King & Stockbarger(1940)[38]	Absorption cell	0.0023	
Webb & Messenger(1944)[56]	Lifetime-phase shift	0.00223	≈ 1.12
Matland(1953)[57]	Lifetime	0.00233 ± 2.4%	
Addink(1959)[33]	Arc emission	0.008	
Geneux & Wanders-Vincenz(1960)[58]	Magnetic dipole resonance	0.00219 ± 3%	
Barrat & Butaux(1961)[59]	Magnetic resonance	0.00212 ± 2-3%	
Corliss & Bozman(1962)[27]	Cu arc emission	0.0014	0.92
Helliwell(1963)[60]	Theoretical: modified SCF	0.00305	1.95
Bieniewski(1964)[61]	Absorption cell	0.00194 ± 10%	
Lurio & Novick(1964)[24]	Level crossing		1.42 ± 3%
Byron et al.(1964)[62]	Magnetic double resonance	0.00200 ± 1.7%	
Spitzer(1965)[63]	Level crossing		1.02
Lvov(1965)[64]	Absorption tube		1.3
Moise(1966)[65]	Absorption cell	0.00205	
This investigation (1967)	Atomic beam absorption	0.00190 ± 7%	1.38 ± 12%

pressure of cadmium has been accurately measured, alleviating the major source of error in absorption cell measurements. For these reasons, this is one of the most accurately determined of f-values of lines in complex spectra. Despite the experimental difficulties in measuring this line with the atomic beam, the value obtained agrees within experimental error with the results of other methods.

The value obtained for the λ2288 line agrees with the recent level crossing work of Lurio and Novick[24] and the absorption cell measurement of Lvov.[64] Other values are generally smaller.

Gold: Measurements of the f-value of the gold line λ2428 are given in Table IX. Only 4 of these can make any claim of precision: the hook measurement of Penkin and Slavenas,[40] the absorption cell measurement of Moise,[45] the level crossing measurement of Levin and Budick,[48] and the present atomic beam measurement. The agreement of these values is not good.

The level crossing and atomic beam measurements should be expected to give the most reliable values since they are not dependent on vapor pressure measurements. Unfortunately, it is difficult to compare these values. The level crossing experiment yields the lifetime of the upper state ($^2P^o_{3/2}$) which Levin and Budick found to be 5.3×10^{-9} sec $\pm$ 19%. Because of the transitions λλ3123,5065 to the $^2D_{5/2,3/2}$ states, the branching ratio to the $^2S_{1/2}$ ground state is needed. This can be obtained if either relative f-values for all the transitions or absolute f-values for the λλ3123,5063 transitions are

Table IX Oscillator strengths for Au λ2428

Observer	Method	f-value
Addink(1959)[33]	Arc emission	0.035
Corliss & Bozman(1962)[27]	Cu arc emission	0.08
Penkin & Slavenas(1963)[40]	Hooks	0.41 ± 7%
Lawrence,Link, & King(1965)[11]	Atomic beam absorption	> 0.15
Moise(1966)[45]	Absorption cell	0.18 ± 11%
Levin & Budick(1966)[48]	Level crossing	0.24 ± 38%*
This investigation (1967)	Atomic beam absorption	0.283 ± 5.3%

* See text

known. The only values available are the copper arc values of Corliss and Bozman.[27] They give $f_{\lambda 2428} = 0.08$, $f_{\lambda 3123} = 0.045$, and no value for λ5065. An estimate can be made for λ5065 by comparing the f-values for the analogous multiplet of copper. The result is $f_{\lambda 5065} = 0.023$, which is fortunately small enough that a relatively large error in its value may be tolerated compared to errors in the other f-values.

If these f-values are treated as relative f-values, the branching ratio is $0.465 \pm 30\%$ (error derived from factor of error of 1.4 quoted by Corliss and Bozman for their relative values), and the f-value for λ2428 derived from Levin and Budick's lifetime value is $0.155 \pm 36\%$.

However, the f-values of Corliss and Bozmann for the resonance doublet λλ2428,2676 are clearly wrong (both absolutely and relatively), probably because of self-absorption in the arc. Hence, it may be better to use the f-values for λλ3123,5065 as absolute values. If this is done, the f-value derived from the lifetime is $0.241 \pm 38\%$ (error calculated from factor of error of 1.9 quoted by Corliss and Bozman for absolute values). This value is quoted in Table IX.

Clearly it is not possible at this time to make a meaningful comparison of the atomic beam value and the level crossing value.

The comparisons of the atomic beam measurements and other reliable measurements for the Cu line λ3247 and the Cd line λ3261 show agreement within experimental errors. It therefore is reasonable to expect that the other f-values measured with the atomic beam are also accurate.

APPENDIX

DEPOSIT RATE FOR CORRECTIONS

Several possible mechanisms are listed in Section II-H which can cause the observed deposit rate to differ from the value it should have corresponding to the density of the atomic beam. These mechanisms are: (1) Non-constant atomic beam flux, (2) The presence of molecules of the element being studied in the atomic beam, (3) Non-unity sticking coefficient of the atoms on the pan, and (4) Adsorption of residual gas by the deposit. In each case discrepancies also appear in the recovery times which permit the data to be either corrected or discarded.

In the following, let G^{true} be the "correct" deposit rate and G^{obs} the observed rate.

If the atomic beam density is varying slowly with time, the observed deposit rate will generally vary also. However, G^{obs} contains not only the rate at which the mass of the pan increases (G^{true}) but also a term proportional to the time derivative of the impulse force. This can be written

$$G^{obs} = G^{true} - \frac{1}{g}\frac{d\mathcal{F}}{dt}$$

$$= G^{true} - t_R \frac{dG^{true}}{dt} \qquad \text{(A-1)}$$

where the recovery time t_R is defined to be $1/g$ times the ratio of the impulse force $\mathcal{F}$ and the true deposit rate G^{true}. At a given

temperature t_R is a constant given by equation (42).

The solution of equation (A-1) is

$$G^{true} = -\frac{e^{t/t_R}}{t_R} \int G^{obs}\ e^{-t/t_R}\ dt + A\ e^{t/t_R} \qquad (A\text{-}2)$$

where A is a constant of integration. It is possible for G^{true} to vary in such a way that G^{obs} remains constant. In this case G^{true} must be given by

$$G^{true} = G^{obs} + A\ e^{t/t_R} \qquad (A\text{-}3)$$

For a typical f-value measurement the shutter under the microbalance pan is opened $\approx 2t_R$ before W_λ is measured and closed $\approx 2t_R$ afterward. The recovery time is measured on opening and closing the shutter. If these two measurements differ by 10%, then the difference between G^{obs} and G^{true} is 1.4% at the time W_λ is measured. It is clear that it is impossible for a significant fluctuation in G^{true} to go unnoticed; either G^{obs} will fluctuate or there will be a large difference in the t_R's. In practice, such data is either discarded or given a low weight. Thus, mechanism (1) is unimportant.

Some elements do not vaporize to a pure monatomic gas, but instead the vapor also contains diatomic, triatomic, and/or higher mass molecules. In this case, equations (34) and (40) can be applied to each type of molecule with M replaced by nM for a molecule of n atoms. If the relative amounts of the various molecules are known,

the separate parts of G and $\mathcal{F}$ can be added up to give the observed values G^{obs} and $\mathcal{F}^{obs}$ and the observed recovery time t_R^{obs} can be found from their ratio.

In practice the relative amounts are not known. The best that can be done is to assume that there is one kind of molecule (probably diatomic) in addition to the atoms. Then, if G^{true} is the deposit rate due to the atoms and αG^{true} is the deposit rate due to the molecules, the observed deposit rate and impulse force are

$$G^{obs} = (1 + \alpha)\, G^{true} \qquad (A\text{-}4)$$

and

$$\mathcal{F}^{obs} = \left(1 + \frac{\alpha}{\sqrt{n}}\right) \mathcal{F}^{true} \quad . \qquad (A\text{-}5)$$

The observed recovery time is

$$t_R^{obs} = \frac{\mathcal{F}^{obs}}{gG^{obs}} = \left(\frac{1 + \alpha/\sqrt{n}}{1 + \alpha}\right) t_R^{th} \qquad (A\text{-}6)$$

where t_R^{th} is the recovery time for $\alpha = 0$ and is given by equation (42).

Equation (A-6) can be solved for α:

$$\alpha = \frac{1 - (t_R^{obs}/t_R^{th})}{\Lambda + (t_R^{obs}/t_R^{th})} \qquad (A\text{-}7)$$

with

$$\Lambda = -1/\sqrt{n} \quad . \qquad (A\text{-}8)$$

Now equation (A-7) can be substituted into equation (A-4) to give the relation between the observed and true deposit rates:

$$G^{true} = F_G \, G^{obs} \qquad \text{(A-9)}$$

with

$$F_G = 1 - \left(\frac{1}{1+\Lambda}\right)\left(1 - t_R^{obs}/t_R^{th}\right) \quad . \qquad \text{(A-10)}$$

And so, for the case of n-atomic molecules in the atomic beam, the deposit rate correction is given by the observed recovery time as described in Section II-H.

The other two mechanisms, non-unity sticking coefficient and gas adsorption, can be treated together. Consider the following situation. The atomic beam consisting of atoms of mass M is impinging on the pan from the below, and residual gas in the vacuum chamber consisting of molecules of mass M_A is impinging on both the top and the bottom of the pan. Atoms (or molecules) of mass M_B are being emitted from the bottom of the pan, and the residual gas is bouncing off the top. Only that fraction of the residual gas which is adsorbed if it strikes the deposit will be counted since gas that bounces off both sides of the pan has no observable effect. However, because of the impulse force it imparts, it is important to include the residual gas hitting the top of the pan which corresponds to the gas being adsorbed on the bottom.

It will now be assumed that the distribution of residual gas atoms hitting the top or bottom of the pan is the same as it would be

if the pan were a flat plate, though in fact it is conical. This distribution is then similar to that given by equation (1) for atoms effusing out of the orifice to form the atomic beam; i.e. the number of molecules per second hitting the pan at an angle θ from the normal, per unit solid angle, per unit speed interval, is

$$\mathcal{N}^{A}{}_{v}(\theta) = K_A \beta_A^3 v^3 e^{-\beta_A^2 v^2} \cos\theta \qquad \text{(A-11)}$$

with

$$\beta_A = \sqrt{M_A/2RT_A} \qquad \text{(A-12)}$$

where T_A is the ambient temperature and K_A is a constant. Similarly, molecules leaving the pan will have the same type of distribution except that T_A will be replaced by the temperature of the pan T_p.

As before, the deposit rate and impulse force due to the atomic beam are related by

$$\mathcal{I}^{true} = g\, t_R^{th}\, G^{true} = \frac{3\sqrt{\pi}}{4\beta} G^{true} \,. \qquad \text{(A-13)}$$

The deposit rate due to the residual gas impinging on one side of the pan is

$$G_A = \frac{M_A}{N_o} \int_0^\infty dv \int_{2\pi} d\Omega \; \mathcal{N}^{A}{}_{v}(\theta)$$

$$= \frac{\pi M_A K_A}{2 N_o \beta_A} \,. \qquad \text{(A-14)}$$

The corresponding impulse force is

$$\mathcal{F}_A = \frac{M_A}{N_o} \int_0^\infty dv \int_{2\pi} d\Omega \; v \cos\theta \; \mathcal{N}^A{}_v(\theta)$$

$$= \frac{\pi^{3/2} M_A K_A}{4 N_o \beta_A{}^2}$$

$$= \frac{\sqrt{\pi}}{2 \beta_A} G_A \quad . \tag{A-15}$$

Let

$$G_A = \alpha_A G^{true} \quad . \tag{A-16}$$

Then, combining equations (A-13) and (A-16), we have

$$\mathcal{F}_A = \alpha_A \frac{2}{3} \frac{\beta}{\beta_A} \mathcal{F}^{true}$$

$$= \alpha_A \frac{2}{3} \sqrt{(T_A/T)(M/M_A)} \; \mathcal{F}^{true} \quad . \tag{A-17}$$

Similarly, for the atoms bouncing off the top of the pan,

$$G_A' = \alpha_A G^{true} \tag{A-18}$$

and

$$\mathcal{F}_A' = \alpha_A \frac{2}{3} \sqrt{(T_p/T)(M/M_A)} \; \mathcal{F}^{true} \quad . \tag{A-19}$$

And for the atoms emitted from the bottom of the pan,

$$G_B' = \alpha_B G^{true} \tag{A-20}$$

and

$$\mathcal{I}_B' = \alpha_B \frac{2}{3} \sqrt{(T_p/T)(M/M_B)} \; \mathcal{I}^{true} \quad . \tag{A-21}$$

Now the individual deposit rates and impulse forces can be added to give the observed values:

$$G^{obs} = G^{true} + G_A + G_A - G_A' - G_B' \tag{A-22}$$

and

$$\mathcal{I}^{obs} = \mathcal{I}^{true} + \mathcal{I}_A - \mathcal{I}_A - \mathcal{I}_A' + \mathcal{I}_B' \, , \tag{A-23}$$

or

$$G^{obs} = [\, 1 + \alpha_A - \alpha_B \,] \, G^{true} \tag{A-24}$$

and

$$\mathcal{I}^{obs} = [\, 1 - \tfrac{2}{3} \sqrt{T_p/T} \, (\alpha_A \sqrt{M/M_A} - \alpha_B \sqrt{M/M_B}) \,] \; \mathcal{I}^{true} \quad . \tag{A-25}$$

The observed recovery time is obtained from the ratio of equations (A-25) and (A-24):

$$t_R^{obs} = \left[\frac{1 - \frac{2}{3} \sqrt{T_p/T} \, (\alpha_A \sqrt{M/M_A} - \alpha_B \sqrt{M/M_B})}{1 + \alpha_A - \alpha_B} \right] t_R^{th} \quad . \tag{A-26}$$

With this result, the separate mechanisms can be treated. For non-unity sticking coefficient, no atoms of residual gas are involved so $\alpha_A = 0$, and the atoms emitted by the deposit are the same as those in the atomic beam so $M_B = M$. To be consistent with equations (A-4), let $\alpha = -\alpha_B$. With these values, equation (A-26) can be solved for α. The result is equation (A-7) with

$$\Lambda = \frac{2}{3}\sqrt{T_p/T} \quad , \tag{A-27}$$

and the deposit rate correction is given by equations (A-9) and (A-10).

For adsorbed gas, we have $\alpha_B = 0$ and $\alpha = \alpha_A$. Equations (A-7), (A-9), and (A-10) are again valid but with

$$\Lambda = \frac{2}{3}\sqrt{(T_p/T)(M/M_A)} \quad . \tag{A-28}$$

If the residual gas reacts with the deposit, releasing another gas, this can also be handled using equation (A-26). If each incoming molecule of mass M_A produces one outgoing molecule of mass M_B, then $\alpha_B = (M_B/M_A)\alpha_A$, $\alpha = \alpha_A - \alpha_B$, and

$$\Lambda = \frac{2}{3}\sqrt{T_p/T}\left[\frac{\sqrt{M}}{\sqrt{M_A}+\sqrt{M_B}}\right] . \tag{A-29}$$

The range of values of Λ and $1/(1+\Lambda)$ for the various mechanisms is given in Table X. It can be seen that, except for the case of molecules in the beam, the value of $1/(1+\Lambda)$ is not very sensitive to either the kind of anomaly or the various values of mass and temperature.

Table X Deposit rate correction factors

Cause of anomaly	Λ	$\frac{1}{1+\Lambda}$
Molecules $n = 2$	-0.7071	3.414
$n = 3$	-0.5773	2.366
$n = 4$	-0.5000	2.000
$n = 6$	-0.4082	1.690
Sticking coefficient		
$T = 2300\ ^{o}K$, $T_p = 500\ ^{o}K$	0.311	0.763
$T = 1500\ ^{o}K$, $T_p = 500\ ^{o}K$	0.385	0.722
$T = 500\ ^{o}K$, $T_p = 300\ ^{o}K$	0.516	0.659
Adsorption of H_2O ($M_A = 18$)		
Fe: $T = 2300\ ^{o}K$, $T_p = 500\ ^{o}K$	0.548	0.646
Cd: $T = 500\ ^{o}K$, $T_p = 300\ ^{o}K$	1.290	0.437
Au: $T = 2000\ ^{o}K$, $T_p = 500\ ^{o}K$	1.103	0.476

Cadmium offered an opportunity to test the sticking coefficient correction. Four f-value measurements were made before the pan was cleaned with the heater (see Section IV-C). The sticking coefficient during these scans ranged from 20% to 70%, yet the corrected f-values were not significantly different than the results of measurements made when the sticking coefficient was nearly unity.

For the mechanism of gas adsorption, it has been tacitly assumed that the adsorption occurs only when the atomic beam is

depositing on the pan and stops immediately when the shutter is closed. Since the time to form a monolayer is less than 2 sec at pressures greater than 10^{-6} torr, it is possible for this to be approximately true. However, the other extreme, adsorption continuing for long periods after the shutter is closed, is also possible. In this case the adsorption appears as a constant drift which is easily subtracted off.

The worst case is when the adsorption dies away in a time comparable to the recovery time. In this case the deposit rate recording is difficult to interpret. This commonly occurs when the pan heater is not used, thus spoiling what would otherwise be a good test of the gas adsorption correction.

As it turned out, the correction for gas adsorption was only needed for gold and then only when the pressure in the vacuum chamber became rather high. In this situation, it is probably valid to assume that the adsorption ceases when the atomic beam is intercepted by the shutter.

REFERENCES

1. Foster, E. W., Rpts. Progr. in Phys. 27, 469 (1964).
2. Wessel, G., Z. Physik 126, 440 (1949).
3. Kopfermann, H. and Wessel, G., Z. Physik 130, 100 (1951).
4. Davis, M. H., Ph.D. Thesis, California Institute of Technology (1955).
5. Bell, G.D., Ph.D. Thesis, California Institute of Technology (1957).
6. Bell, G. D., Davis, M. H., King, R. B., and Routly, P. M., Astrophys. J. 127, 775 (1958).
7. Bell, G. D., Davis, M. H., King, R. B., and Routly, P. M., Astrophys, J. 129, 437 (1959).
8. Bell, G. D. and King, R. B., Astrophys. J. 133, 718 (1961).
9. Lawrence, G. M., Ph.D. Thesis, California Institute of Technology (1963).
10. Link, J. K., Ph. D. Thesis, California Institute of Technology (1963).
11. Lawrence, G. M., Link, J. K., and King, R. B., Astrophys. J. 141, 293 (1965).
12. Kennard, E. H., Kinetic Theory of Gases (McGraw-Hill Book Company Inc., New York, 1938).
13. Unsöld, A., Physik der Sternatmosphären, 2nd Ed. (Springer-Verlag, Berlin, 1955).

14. Aller, L. H., Astrophysics: The Atmospheres of the Sun and Stars, 2nd Ed. (Ronald Press Company, New York, 1963).

15. Moise, N. L., Ph.D. Thesis, California Institute of Technology (1963).

16. Stahl, H. A., J. Opt. Soc. Am. 49, 381 (1959).

17. Strong, J. (ed.), Procedures in Experimental Physics (Prentice-Hall, Inc., New York, 1938).

18. Krasha, M., J. Opt. Soc. Am. 38, 929 (1948).

19. Nesmeyanov, An. N., Vapour Pressure of the Elements (Translator, Carasso, J. I., Academic Press, New York, 1963).

20. Brix, P. and Kopfermann, H., Landolt-Börnstein Zahlenwerte und Funktionen, 6th Ed., Vol. I, Part 5, 1-69 (ed. Eucken, A., Springer-Verlag, Berlin, 1952).

21. Kelly, F. M. and Tomchuk, E., Proc. Phys. Soc. (London) 74, 689 (1959).

22. Kelly, F. M. and Tomchuk, E., Proc. Phys. Soc. (London) 78, 1304 (1961).

23. Kuhn, H. G. and Ramsden, S. A., Proc. Roy. Soc. (London) A237, 485 (1956).

24. Lurio, A. and Novick, R., Phys. Rev. 134, A608 (1964).

25. Procter, W. G., Phys. Rev. 79, 35 (1950).

26. Elliott, R. M. and Wulff, J., Phys. Rev. 55, 170 (1939).

27. Corliss, C. H. and Bozman, W. R., Experimental Transition Probabilities for Spectral Lines of Seventy Elements (National Bureau of

Standards Monograph 53, U. S. Government Printing Office, Washington, D.C., 1962).

28. Allen, C. W. and Corliss, C. H., Monthly Notices Roy. Astron. Soc. 126,37 (1963).

29. King, R. B., Astrophys. J. 95, 78 (1942).

30. Allen, C. W. and Asaad, A. S., Monthly Notices Roy. Astron. Soc. 117,36 (1957).

31. Hinnov, E. and Kohn, H., J. Opt. Soc. Am. 47, 156 (1957).

32. Ziock, K., Z. Physik 147, 99 (1957).

33. Addink, N. W. H., Spectrochim. Acta 15, 349 (1959).

34. Ottinger, C. and Ziock, K., Z. Naturforsch. 16A, 720 (1961).

35. Morozova, N. P. and Startsev, G. P., Optics and Spectroscopy (U.S.S.R.) 17, 174 (1964).

36. Corliss, C. H. and Warner, B., Astrophys. J. Suppl. Ser. 8, No. 83, 395 (1964).

37. Corliss, C. H. and Warner, B., J. Research Natl. Bur. Standards 70A, 325 (1966).

38. King, R. B. and Stockbarger, D. C., Astrophys. J. 91, 488 (1940).

39. Ostrovskii, Yu. I. and Penkin, N. P., Optika i Spektroskopiya 3, 193 (1957).*

---

* English translation available in Optical Transition Probabilities, A Collection of Russian Articles, 1924-1960 (National Science Foundation, Washington, D.C., and Department of Commerce, U.S.A. by the Israel Program for Scientific Translations, Jerusalem, 1962).

40. Penkin, N. P. and Slavenas, I. Yu. Yu., Optics and Spectroscopy (U.S.S.R.) 15, 3 (1963).

41. Vidale, G. L., Technical Information Series Report R60SD331, General Electric Company, Space Sciences Laboratory (1960).

42. Riemann, M.,Z. Physik 179, 38 (1964).

43. Stewart, J. C., and Rotenberg, M., Phys. Rev. 140, 1508A (1965).

44. Ostroumenko, P. P. and Rossikhin, V. S., Optics and Spectroscopy (U.S.S.R.) 19, 365 (1965).

45. Moise, N. L., Astrophys, J. 144, 774 (1966).

46. Slavenas, I. Yu. Yu., Optics and Spectroscopy (U.S.S.R.) 20, 264 (1966).

47. Ney, J., Z. Physik 196, 53 (1966).

48. Levin, L. A. and Budick, B., Bull. Am. Phys. Soc. 11, 455 (1966).

49. Cunningham, P. and Link, J. K.(to be published in J. Opt. Soc. Am.).

50. Kuhn, W., Naturwissenschaften 14, 48 (1926).

51. Soleillet, P., Compt. rend. 187, 212 (1928).

52. Ellett, A., Phys. Rev. 33, 124 (1929).

53. Zemansky, M. W., Z. Physik 72, 587 (1931).

54. Koenig, H. D. and Ellett, A., Phys. Rev. 39, 576 (1932).

55. Soleillet, P., Compt. rend. 196, 1991 (1933).

56. Webb, H. W. and Messenger, H. A., Phys. Rev. 66, 77 (1944).

57. Matland, C. G., Phys. Rev. 91, 436 (1953).

58. Geneux, E. and Wanders-Vincenz, B., Helv. Phys. Acta 33, 185 (1960).

59. Barrat, J. P. and Butaux, J., Compt. rend. 253, 2668 (1961).

60. Helliwell, T. M., Ph.D. Thesis, California Institute of Technology (1963).

61. Bieniewski, T., Monthly Notices Roy. Astron. Soc. 127, 359 (1964).

62. Byron, Jr., F. W., McDermott, M. N., and Novick, R., Phys. Rev. 134, A615 (1964).

63. Spitzer, M., Compt. rend. 260, 3907 (1965).

64. Lvov, B. V., Optics and Spectroscopy (U.S.S.R.) 19, 282 (1965).

65. Moise, N. L., Astrophys. J. 144, 763 (1966).